POTENTIAL EFFECT OF RIVER BATHYMETRY ON RIVERINE FLOOD SIMULATION AT WATERSHED SCALE

by

MARIAM KHANAM

SAGY COHEN, COMMITTEE CHAIR
SARAH PRASKIEVICZ
NATASHA DIMOVA

A THESIS

Submitted in partial fulfillment of the requirements
for the degree of Master of Science
in the Department of Geography
in the Graduate School of
The University of Alabama

TUSCALOOSA, ALABAMA

2018

Copyright Mariam Khanam 2018
ALL RIGHTS RESERVED

ABSTRACT

Flood prediction and mitigation systems are invaluable for improving public safety and community resilience worldwide. Hydrologic and Hydraulic (H & H) simulation of flood eventsis becoming an increasingly efficient tool for studying and predicting flood events and susceptibility. A consistent limitation of H & H simulations of riverine dynamics is the lack of information about river bathymetry as most terrain data record the water surface elevation over a stream. The impact of this limitation on the accuracy of simulations of the flood has not been well studied over a large range of flood magnitudes and modeling frameworks. Advancing our understanding of this topic is timely, given emerging national and global efforts for developing automated flood prediction systems (e.g. NOAA National Water Center). Here, I study the response of flood simulation to the incorporation of hydraulic geometry derived bathymetry. GSSHA, a distributed 2D hydrologic/hydraulic model with the capability of 1D routing was used as a simulation tool. I test a hypothesis that the impact of inclusion/exclusion of bathymetry data on the model results will vary in its magnitude as a function of river size and flood magnitude. This will allow researchers and stakeholders to better predict flood hazards, benefiting communities in a vulnerable flood zone.

DEDICATION

I dedicate this thesis to every person who mentored me and helped me unfold the attainments of life including this manuscript. Most explicitly, my supportive family members without whom I wouldn’t be where I am today.

ACKNOWLEDGMENTS

I want to express my earnest gratitude to my advisor Dr. Sagy Cohen for his perpetual help, support, advice and motivation during the past two years of my master tenure. The planning and execution of this thesis research were only possible because of Dr. Cohen's expert guidance and a generous supply of well-equipped lab with technology and responsive environment.

I would also like to thank my thesis committee members, Dr. Sarah Praskievicz and Dr. Natasha Dimova for their contribution to help me articulate a well-structured scientific document. Specially, I want to convey my regards to Dr. Sarah whom I found available for advice and answering my queries. A very special thanks to Dr. Zhe Li, NOAA affiliate at National Water Center for helping me with the bathymetry data. I am grateful for the funded position throughout my MS tenure to Dr. Cohen again and the department.

CONTENTS

LIST OF TABLES

LIST OF FIGURES

CHAPTER 1

INTRODUCTION

Climate change and human interference have altered the frequency and intensity of hydrologic events like precipitation and floods, yielding vulnerability for communities dwelling in coastal regions and within inland floodplains (EPA, 2015). Extensive desolation, economic hazard and loss of lives due to extreme precipitation induced flood events are intensifying gradually (Zhong et al. 2014; Bowering et al., 2014; Tripathi et al., 2014). Flood prediction and mitigation schemes are therefore necessary for improving public safety and community resilience worldwide at country, continental and global scales.

Flood hazard mapping using numerical models for studying and predicting flood events and susceptibility has increased considerably in recent years. As an example, in 2016 the National Oceanic and Atmospheric Administration (NOAA) National Water Center (NWC) has released the National Water Model (NWM) as part of their effort to develop a hyper-resolution national-scale flood prediction system for the U.S. The NWM is a hydrology model that predicts streamflow in over 2.7 million river, stream and canal reaches across the U.S. The planned NWC flood prediction system will include a procedure for translating NWM streamflow prediction to flood inundation predictions, using hydraulic and hydrologic models and topographic analysis. In a parallel effort, the Federal Emergency Management Agency (FEMA) uses numerical models as one of its tools to produce maps for the National Flood Insurance Program (NFIP).

Globally, examples of the use of numerical models for flood prediction and analysis include the European Exchange Circle on Flood Mapping's (EXCIMAP) approach to produce

flood maps for over 24 European countries (Martini & Loat, 2007) and Japan's repository of flood maps for 180 rivers from 1995 to 2004 (Zhong et al., 2014; Liu, 2005; Wang, 2005). China, Britain, Norway, Canada, Australia and other countries have also produced flood risk maps using numerical model simulations (Zhong et al., 2014; Ma, et al., 2005; Rooke, 2005).

Flood maps are widely used as a primary planning and action tool in all phases of an extreme event to strategize evacuations, stage emergency response and conduct damage control. Given the demand and importance of simulation-based flood maps, the accuracy of flood mapping is crucial. One of the major challenges in two-dimensional hydrologic and hydraulic modeling is to accurately represent river channel and floodplain geometries. There are several techniques for deriving river bathymetry data. Modern hydrologic modeling systems use either high spatial resolution LiDAR DEMs, observed river bathymetry data or empirically derived geometries (refs.).

Bathymetry and detailed floodplain topography data are not readily available for most rivers. There are several sources (e.g. NED, SRTM, LiDAR) from which DEMs of different resolutions can be obtained. The increased availability of high-resolution DEMs (e.g. LiDAR data) alleviates this challenge for floodplains, but with the exception of blue/green LiDAR surveys, these do not reflect the river bathymetry, only the water-surface elevation. However, blue/green LiDAR surveys are very expensive and less reliable while encountering increasing depth and turbulence in the water (Gao, 2009; Legleiter & Overstreet, 2012; McKean et al., 2014).

Observed bathymetry data is usually based on surveyed cross-sectional data, collected to analyze the morphology and shape of the river (channel depth, width, and wetted perimeter). The bathymetry data, as well as velocity data, is collected at a particular section of a river along the

width of the river at some pre-defined intervals. The latest technology used in surveying river bathymetry is Acoustic Doppler Current Profiler (ADCP). This instrument applies the principles of sound waves to record data. Survey data can be found for small rivers, but data availability for large rivers is limited.

River channel geometry can be estimated based on three basic parameters: channel length, channel width and bank height (Yamazaki et al., 2011), typically simplified by assuming a trapezoidal channel cross-sectional shape. These parameters can be calculated by a set of power-law empirical equations (Leopold & Maddock, 1953) called "Hydraulic Geometry". Channel geometry equations can also be generated by relating bankfull discharge of a variety of rivers to drainage area (Dudley, 2004).

The selection of the bathymetry and floodplain topography data source typically depends on its availability and, to a lesser extent, on model requirements. However, there is no strong science behind the reason to choose one source over another. Most elevation datasets do not capture the river bathymetry (Cook & Merwade, 2009), and thus provide no information on river depth or bankfull level. Surveyed bathymetry data is relatively rare as it is expensive in time and resources. Hydraulic geometry can be a great alternative to the above datasets and compensate for the scarcity of observational data. Although empirically derived bathymetry and floodplain geometry are based considerably on approximation, using hydraulic geometry data for estimating river bathymetry can be more productive than not considering bathymetry and can produce a detailed and convenient platform for scientific comparison. The detailed bathymetry that can be calculated using hydraulic geometry, generates a continuous synthetic channel network, which is necessary for two- and three-dimensional hydraulic (Merwade *et al*., 2008) as well as hydrologic models.

Cook & Merwade (2009) found that flood extent decreases considerably after incorporating bathymetry in the modeling framework. It can be hypothesized that flood depth and duration will also be affected by incorporating detailed bathymetry data. The effect of geometric description, like the spacing of cross-sections, was found to have a considerable impact on flood simulation results (Cook. & Merwade. 2009; Bates et al., 2002; Werner, 2001; Yu and Lane, 2006). Conventional studies related to bathymetry are not surprisingly restricted to river reach scale study domains as might be assumed based on the paucity of bathymetry data for a large area. A hydraulic or hydrologic model built for a particular river reach illustrates only a localized problem but may not help to understand the overall hydrologic processes. To have a comprehensive picture of hydrologic regime change in a floodplain and river corridor during a flood event, watershed-scale hydrologic models are crucial.

In small rivers and creeks, water surface elevation, captured by standard DEMs, may not considerably differ from river bed elevation, meaning that incorporating detailed bathymetry may have a relatively little effect on simulation results. In large rivers, conversely, water surface elevation might considerably differ from river bed elevation, rendering the accurate description of channel geometry difficult. However, the large magnitude associated with most floods in large rivers might overshadow the impact of detailed bathymetry incorporation. Simulating a range of different river segments with varying stream order, width and depth for different magnitudes of flood events can address these uncertainties. Hydrologic modeling of a large watershed can provide a platform for comparing a considerable range of streams.

In this study, the impact of the geometric description of the river channel and floodplain on flood inundation simulation has been evaluated by using the hydrologic/hydraulic modeling framework GSSHA. Most studies suggest that 2D models are compatible to predict the spatial

distribution of flooding, although when it comes to point measurements, 1D modeling can be advantageous (Horritt & Bates, 2002, Bates & De Roo, 2000). As 1D models are computationally efficient compared to 2D models that are capable of modeling complex topography (Moore, 2011), coupling both 1D and 2D models will yield comparatively accurate results. To avoid the conflict of applicability of 1D and 2D models for flood mapping, a coupled 1D/2D modeling platform has been applied to the watershed.

The primary objective of this study was to evaluate the importance of bathymetry integration for flood simulation at a watershed scale for a range of stream orders. It is hypothesized that incorporating bathymetry data will considerably affect simulated flood depth and extent. It is expected that even if the overall basin is not affected hugely because of bathymetry incorporation, changes will be considerable in small and mid-size streams. This study has also compared the impact of bathymetry integration for different storm events of varying intensity. It is anticipated that changes should be minor during a relatively large event.

CHAPTER 2

STUDY BASIN

There were three criteria while choosing the study area: it should be large enough so that flooding in large, medium and small rivers can be evaluated; it should have availability of a discharge gaging station and weather stations at and near the watershed; and it should have availability of satellite based flood maps for the area to evaluate the model accuracy . Careful consideration of the size and proximity to the coast was also applied in order to avoid very long simulation run-times and the complexity associated with coastal-riverine dynamics.

The study basin chosen is the Red Creek Watershed in southern Mississippi, a tributary of the Pascagoula River and a sub-watershed of the HUC 8 Black Basin (Figure 2.1). Red Creek originates in Lamar County and creates a confluence with the Black River before feeding into the Pascagoula River in Jackson County, Mississippi. The basin is sufficiently inland to ensure that the streamflow through the watershed is not affected by tidal fluctuation or storm surge and flooding is only due to excessive rainfall causing overland flow. The watershed was an appropriate case study as it holds all the other selection criteria.

The Red Creek watershed comprises five different stream orders hence varying in length, depth, and width. Figure 2.2 summarizes the description of these reaches. The watershed has a drainage area of 1,246 square kilometers with a land cover dominated by forest (57.5%; Table2.1). Having less of than 1% of the developed land, Red Creek watershed's eco-system holds significance nationally as the largest unimpeded river in the continental United States (Eco-Logic Restoration Services, LLC., 2007). The bulk of Red Creek's flow navigates through

Stone County. According to the FEMA Flood Insurance Study in 2009 for Stone County, the majority of the flood issues in Stone County are caused due to the overflow of Red Creek during the summer, making the watershed an interesting flood study case.

Table 2.1: Percentages of NLCD 2011 land cover types of Red Creek sub-basin

Land cover type	% Cover
Open water	0.9
Developed land	5.0
Barren Land	0.3
Forested land	57.5
Shrub, grassland & herbaceous	21.7
Agricultural land	8.1
Wetland	27.4

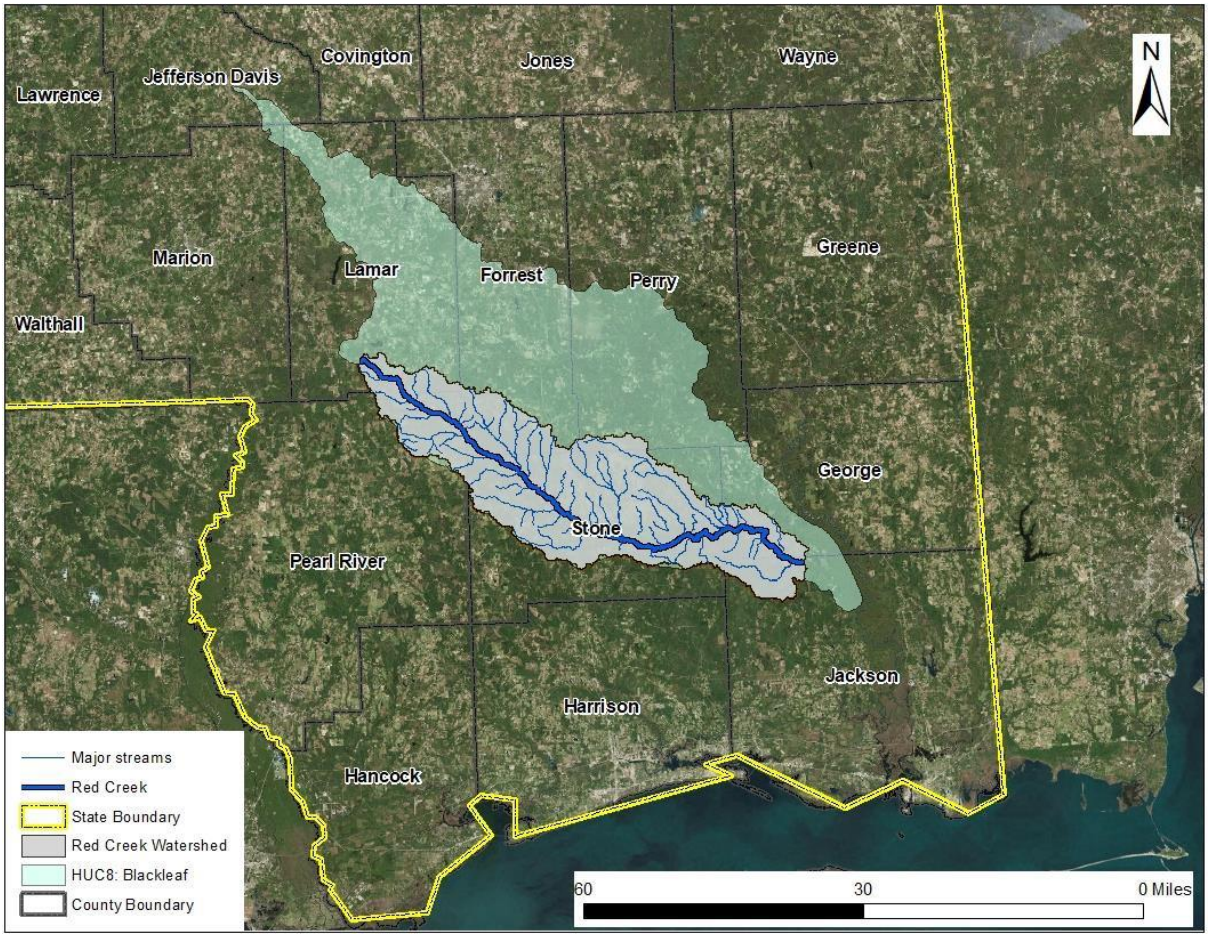

Figure 2.1: Study basin: Red Creek Watershed

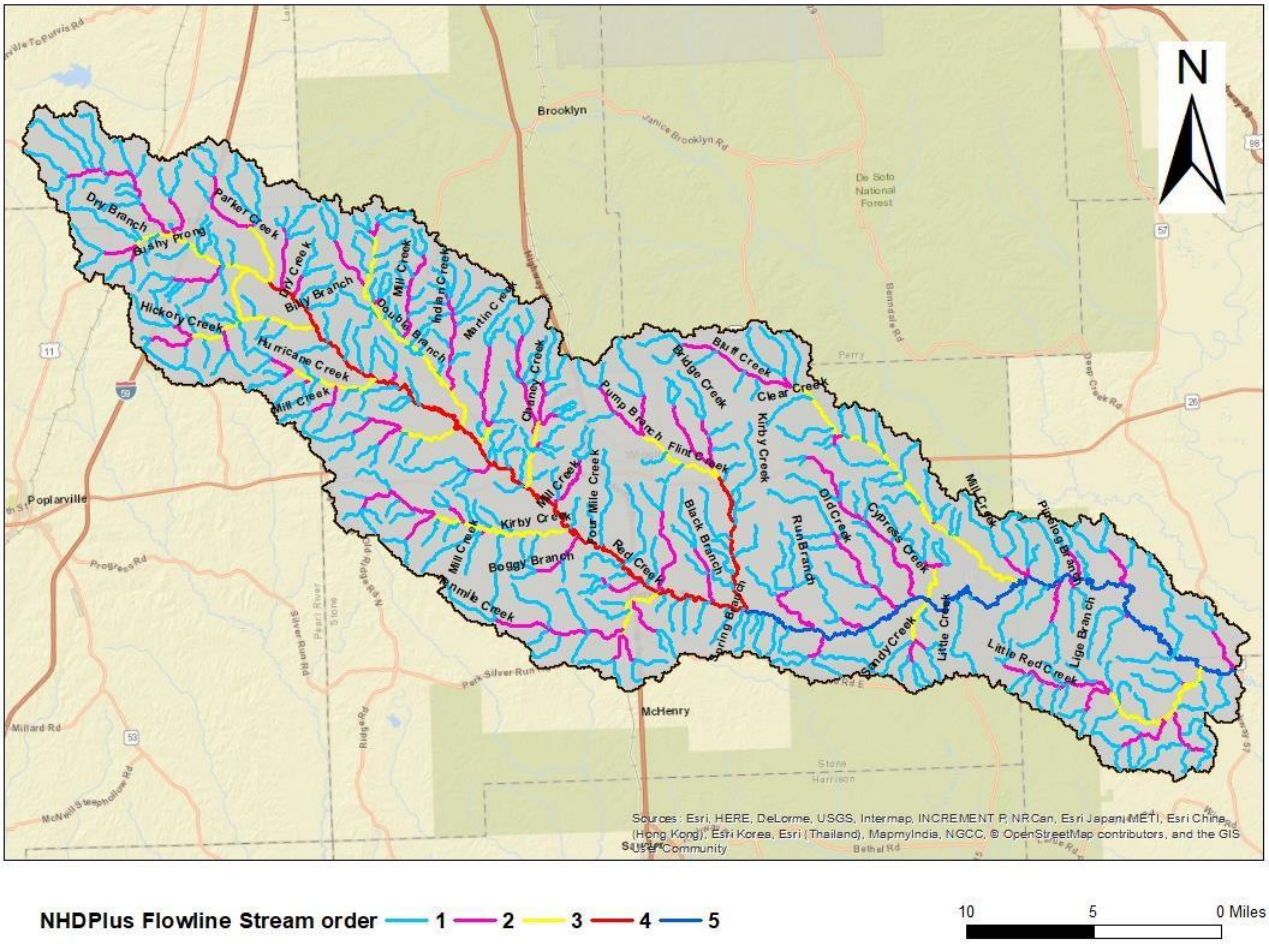

Figure 2.2: Range of stream orders within the Red Creek watershed

CHAPTER 3
METHODOLOGY

3.1 Bathymetry integration

Continuous bathymetry for the study site was generated using the hydraulic geometry approach using the equations developed by Bieger et al. (2015), which relate drainage area to channel dimensions (width, depth and cross-sectional area) for the physiographic regions of the U.S. Bieger et al. (2015) demonstrated that regional hydraulic geometry equations were more reliable over the nationwide equations. The following equation by Bieger et al. (2015) was derived by using bankfull channel parameters:

$$y = aDA^b \quad (1)$$

where *y* is the channel geometry parameter (width, depth or cross-sectional area), *DA* is drainage area (sq km), and *a* and *b* are numerical constants which were derived by Bieger et al. (2015). Bieger et al.'s (2015) suggested values for *a* and *b* were used in the study. Bieger et al. (2015) developed the equations for various physiographic regions. For this study following equations (Table 3.1) for Atlantic Coastal Plain have been used which were derived from 61 sites. (Bieger et al. 2015)

Table 3.1 Hydraulic geometry equations

Geometry parameter	Equation	R^2
Bankful width	$W = 2.22DA^{0.363}$	0.84
Bankful depth	$D = 0.24DA^{0.323}$	0.75
Bankful cross-sectional area	$XA = 0.52DA^{0.68}$	0.84

Channel geometry information was composed by NOAA National Water Center. For all the stream reaches in the study watershed based on the NHDPlus hydrography dataset using the 'NHDPlus Inundation Modeler V5.0 Beta' ArcGIS tool (Li & Clark. 2017). NHDPlus dataset provides information about with for relatively larger streams as a polygon which was used as the bankfull width.

Bathymetry for channel width smaller than 10 m was derived from the 10m NED DEM, simply by subtracting the bankfull depth (derived from the hydraulic geometry equations) from the elevation (assuming uniform depth across the channel). For channel width greater than 10 m, cross-sectional transects were created at a 50m interval along the stream lines. Contrary to the traditional approximation of channel shape as trapezoidal, a quadratic curve (Figure 3.1) was assumed to be the cross-sectional profile. Using Bieger et al. (2015) coefficients the bankfull depth or maximum depth for the quadratic curve at each cross-section was derived. Depth for several points on the quadratic curve was determined using the quadratic equation to generate a full cross-sectional profile at each transect. "Natural Neighbor" interpolation algorithm was applied on the elevations of the sampling points to generate continuous bathymetry for the channel. The bathymetry elevation dataset was then 'burned' into the 10m NED DEM to create a modified DEM with bathymetry information for the channel. Figure 3.2 shows the difference

between the cross-sectional profiles derived from a 10m NED DEM and the modified DEM-with bathymetry information.

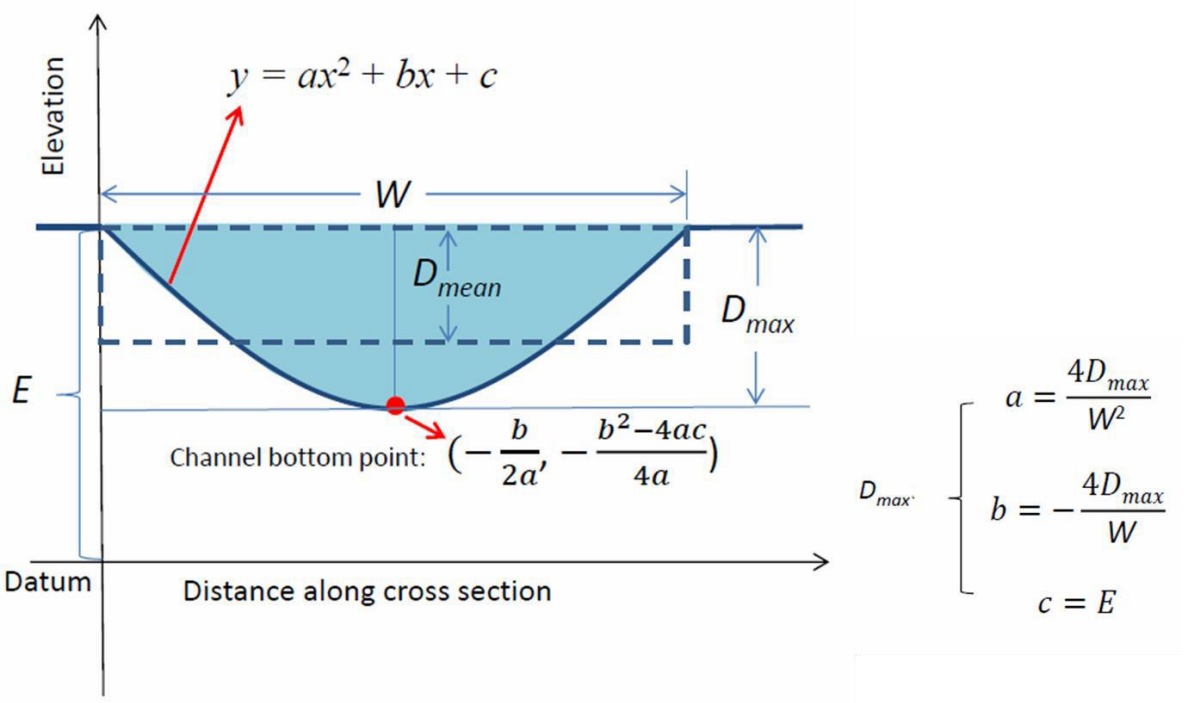

Figure 3.1: Quadratic channel cross-section (produced by Li et al. 2017)

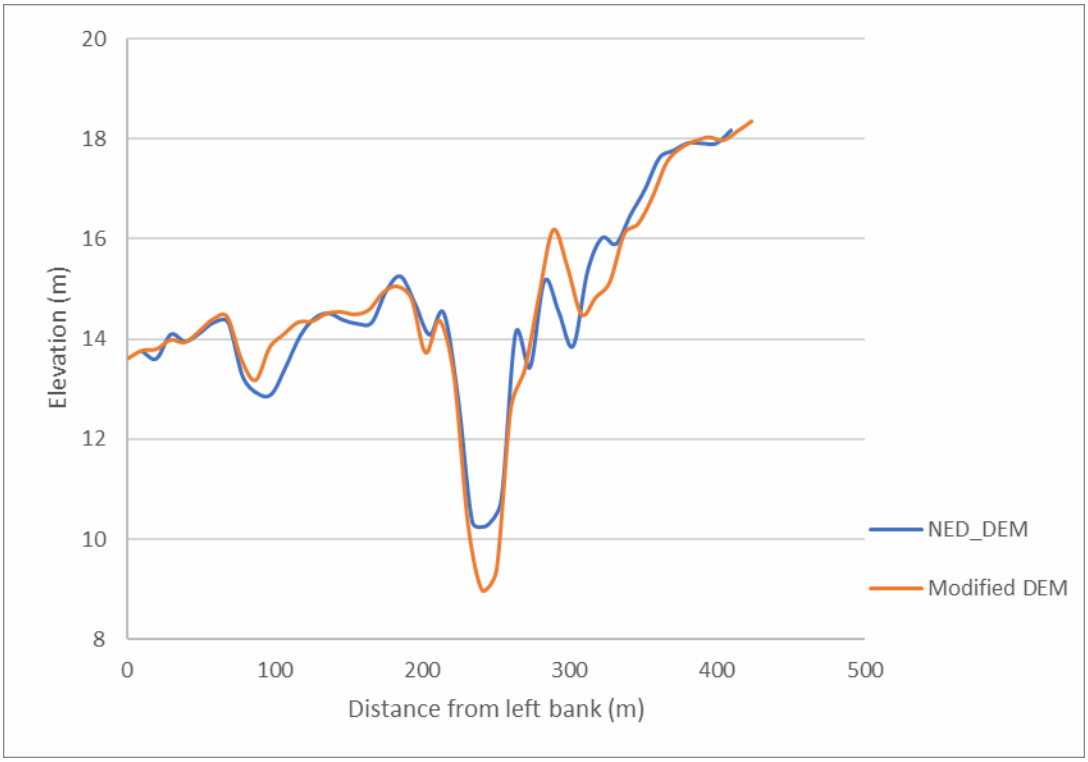

Figure 3.2: Cross-sectional profile comparison at a random stream section

3.2 Hydraulic simulations using GSSHA

GSSHA (Gridded Surface Subsurface Hydrologic Analysis) is a surface and sub-surface hydrologic model facilitated by USACE within the Coastal and Hydraulics Laboratory (CHL) of the U.S. Army Engineer Research and Development Center (ERDC) and developed by Charles W. Downer and Fred L. Ogden. (GSSHA User's manual, 2006) It is a physically based two-dimensional model derived from an earlier hydrologic model CASC2D, also developed by USACE. (GSSHA User's manual, 2006) GSSHA simulates flows, stream depth and soil moisture at a watershed scale using Hortonian and non-Hortonian processes (Downer and Ogden, 2006). GSSHA is based on constant square-grid representation of spatial extent of watershed topography, similar to a DEM. It offers flexibility in computing different hydrologic processes using different approximations. For example: for precipitation distribution, GSSHA

uses Thiessen polygon approximation, for infiltration, Richard's equation, and for evapotranspiration, Penman-Monteith equations can be used (GSSHA, 2017). For 1D channel routing and overland flow routing it approximates a two-step explicit finite volume diffusive wave equation (Downer and Ogden, 2006). Hydraulic structures like weirs, culverts, detention basin can also be incorporated in a model domain (GSSHA, 2017).

In this study, GSSHA simulation was conducted for the study watershed for a series of the storm event (described below), in order to quantify the influence of bathymetry on simulated flooding extent, by running the model with the original DEM (10m NED) and again with the bathymetry-infused DEM.

3.2.1 Setting up the model domain

The model domain was set up for the Red Creek Watershed using both 10 m NED DEM and Modified (bathymetry-infused) DEM. Tools from WMS version 10.1 was used to process the model input and parameter space. WMS Hydrologic modeling wizard uses a method called TOPAZ to computing the flowlines. Flow accumulation threshold for stream delineation was fixed to 1 square mile referring that all the streams having contributing area larger or equal to 1 square mile were delineated. Location of the USGS gaging station 02479300 (Red Creek at vestry, MS) was used as the outlet point of the watershed which resulted in a drainage area of 1,246 km^2. The domain was conditioned for digital dams and pits using GSSHA's Clendam algorithm, a stochastic search process which looks for the most likely flow path connecting a digital dam and a lower elevation (Byrd and Billen 2006; see Sharif et al. 2004). The stream arcs were assigned the properties as generic streams and smoothed to avoid elevation discrepancies along the streamline. A 50x50 m square grid was generated for the whole watershed. This lower spatial resolution (compared to the DEM) was used due to the high computational costs of

simulating a watershed this size. Sharif et al. (2004) demonstrated that using 50 m grid resolution resulted in decent correspondence between the model and observed streamflow compared to other coarser resolution.

For assigning the representative physical properties of the watershed, the Anderson land cover classification (Anderson et al. 1976, GSDA: Land use) United States Department of Agriculture (USDA) dataset and Natural Resources Conservation Service (NRCS) soil type dataset were used. Index tables were created from the land use and soil type coverage. A combined coverage from the land use and soil type was created combining the USDA soil texture and roughness from different land cover (GSSHAwiki). This step is important as the infiltration process of the watershed is highly dependent on the above-mentioned properties. The Green and Ampt equation (GSSHAwiki: Infiltration: Green and Ampt) with soil moisture redistribution process were used as governing infiltration calculation equation.

Evapotranspiration was calculated from the same land cover dataset using Penmann Monteith equation. (GSSHAA user's manual, 2006) The flowlines were assigned as generic streams without setting up any cross-sectional profile for the streams to capture the continuous geometry from both the elevation datasets. As GSSHA does not allow 1D routing for the generic streams, no channel routing scheme was selected during simulation.

3.2.2 Selection of storm events

Precipitation was used as the only source of water into the basin. One of the most important steps of this research was to compile the precipitation input. Initially, the partial frequency distribution curves produced by NOAA was used to construct a design storm and simulate the basin. Designing a synthetic storm event was difficult as it is not representative of a real event which can have either an isolated or a continuous distribution of several high-intensity

peaks. To alleviate this issue, events of different magnitudes were identified from the streamflow records at the USGS gage site. Stream gage rather than rain gage data was used as it was found that, at least for this study site, weather stations often failed to record the rainfall during an extreme event while, stream gaging stations are more reliable in such cases. Moreover, compared to weather stations, frequency analysis of annual maximum peak flow is much easier and more straightforward with stream gaging stations. Frequency analysis is a common procedure to identify the recurrence interval using annual maximum stream flow.

Annual maximum discharge data from 1959-2017 were extracted from the USGS gaging station at the outlet of the Red Creek watershed (Figure 3.3). Log Pearson Type III probability distribution was applied using the following equations to predict the likelihood of extreme discharge event as a function of recurrence interval:

$$\log Q = \overline{\log Q} + K\sigma_{bgx} \quad (2)$$

$$\sigma_{bgx} = \sqrt{\frac{\sum(logQ - \overline{\log Q})^2}{n-1}} \quad (3)$$

$$C_s = \frac{n\sum(logQ - \overline{\log Q})^3}{(n-1)(n-2)(\sigma_{bgx})^3} \quad (4)$$

where Q is the discharge [m^3/s], K is the frequency factor, σ_{bgx} is the standard deviation of all log Q_i and n is the is the number of observations. K is a function of skewness coefficient (Cs) of the dataset (Eq. 3) and recurrence interval which can be found by using Frequency Factor Table (http://streamflow.engr.oregonstate.edu/analysis/floodfreq/skew.htm). K is the key variable for calculating the recurrence interval of an extreme event. After plotting the frequency curve (Figure 3.4), the observed peak annual discharge from different years and dates were tagged with a recurrence interval using the curve. The dates for yearly recurrence intervals of 2, 26 and 47 were selected as these are close to 2, 25 and 50 which are frequently used in hydrological

studies.

Weather stations surrounding the watersheds were investigated for data availability (Table 3) for the dates derived from the frequency analysis of the gaging station. Most of the weather stations data do not date as far back as the stream gaging station. Data from nearby stations (Figure 3.3) helped to alleviate the issue. To account for the water flow travel time from the weather station locations to the stream gage location, partial duration frequency curves by NOAA for the specific weather station were used to validate the cumulative amount of rainfall for an isolated storm event (ref.). The approach taken was to evaluate 15 to 30 days of rainfall data before the identified date in order to find a peak of a certain duration. The value was matched with the NOAA frequency table for justification. For example, for the weather station at Wiggins, the precipitation data (Figure 3.4) for the date 09/7/2011 was selected which has a 2-year recurrence interval. This discrete storm event has a duration of 10 consecutive days with cumulative rainfall of 246.2 mm which coincided with rainfall value of 227 (lower bound: 202, Upper bound: 253) from the NOAA PFDS table which has a partial duration of 10 days and a recurrence interval of 2 years. (https://hdsc.nws.noaa.gov/hdsc/pfds)

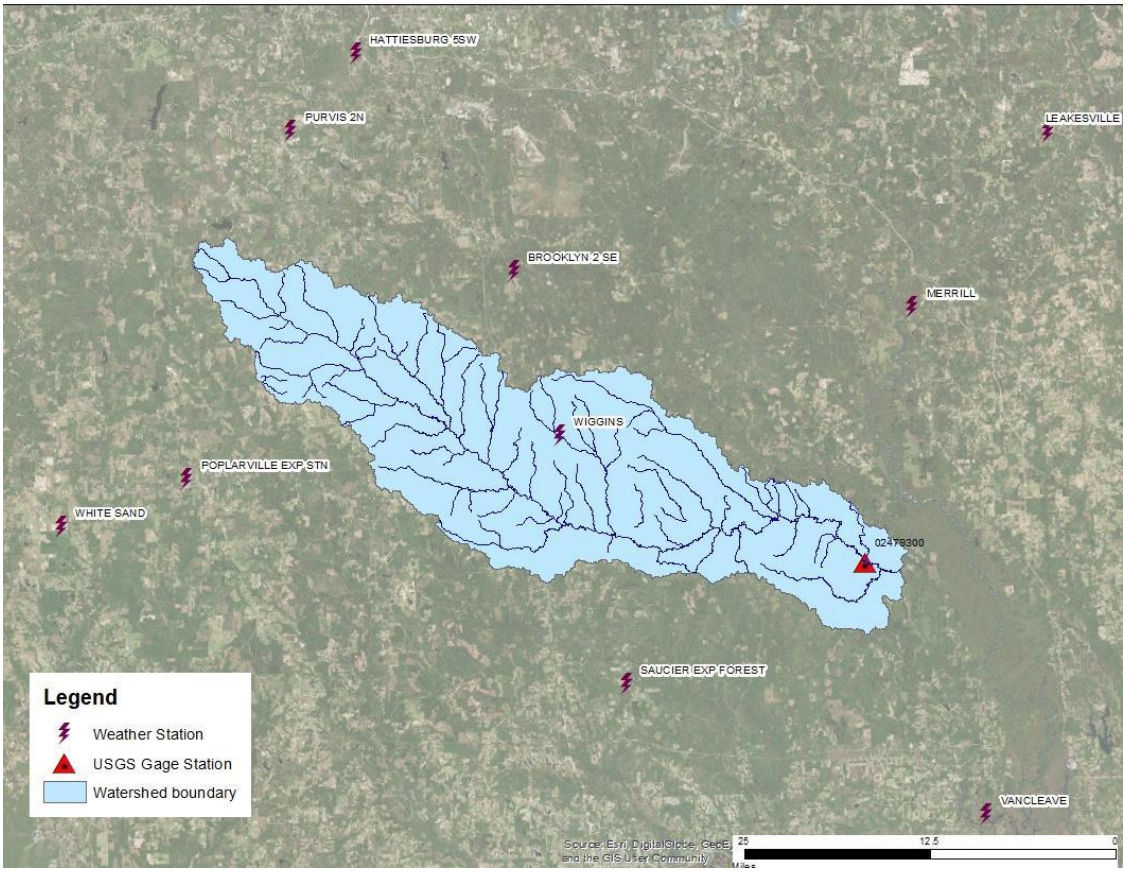

Figure 3.3: Gage station and weather stations for Red Creek watershed

Table 3.2: Date identified for floods in the study site

Date	Gage Height (m)	Peak flow (cms)	Probability (%)	Recurrence interval (years)
8/15/1987	6.5	792.9	2.18	Tr46
9/29/1998	6.4	688.1	3.79	Tr26
9/7/2011	4.7	219.2	62.33	Tr2

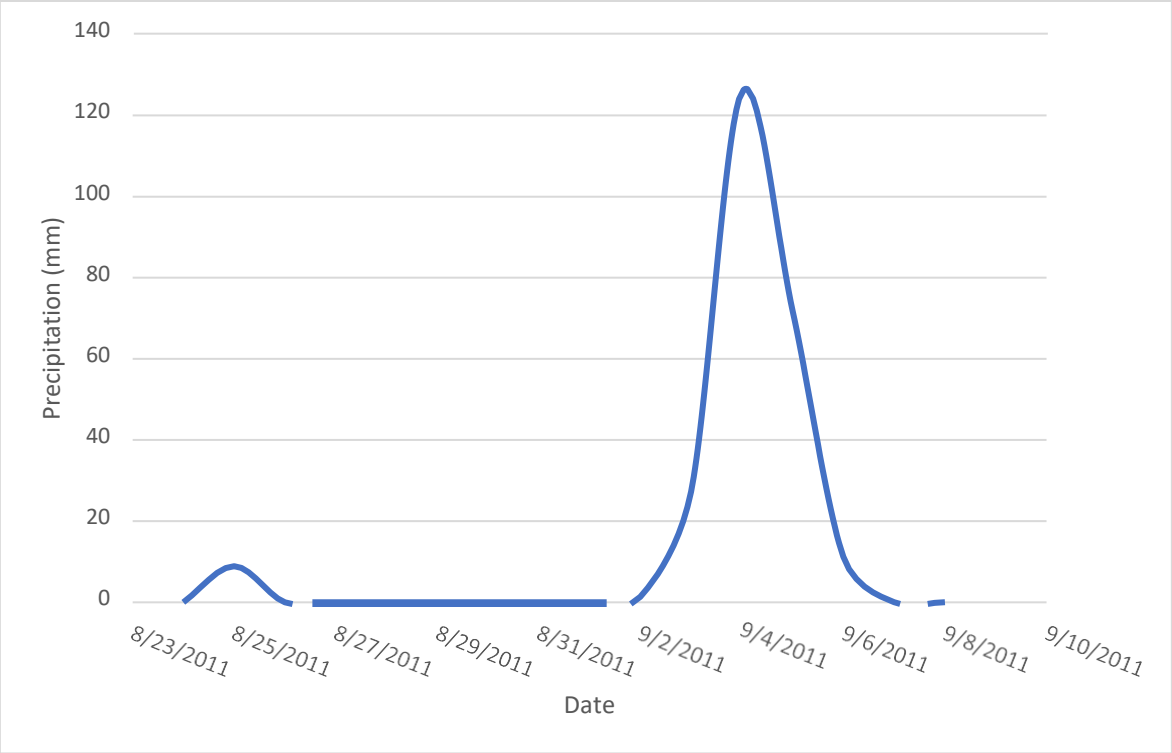

Figure 3.4: Daily rainfall distribution from the weather station at Wiggins

3.2.3 Calibration and validation of the model

Calibration and validation are crucial procedures for establishing robust numerical simulations. Horritt and Bates (2002) suggested that calibrating hydraulic models only against flood extent data is not robust enough, rather use of both flood extent and hydrometry data (e.g. observed discharge) for calibration and validation is useful in differentiating between flood inundation models.

For this study, observed discharge at the outlet was used for calibration of the model and a satellite-derived flood map was used for validation. For validation, flood inundation maps were obtained from the US Flood Inundation Map Repository (USFIMR; http://sdml.ua.edu/usfimr). The flood map from USFIMR is generated using remote sensing of satellite imagery. An individual storm event of 10 days having 1.2 recurrence interval was identified based on the date

of the satellite imagery used by USFIMR. Manual calibration was performed by adjusting the hydrologic parameters and channel roughness values by a stochastic method in GSSHA until the outlet hydrograph (Figure 3.5) was comparable with observed discharge at the USGS gage station. Evidently, the two hydrographs are not very similar, this can be due to the reason that the spatial distribution of the rainfall data was assumed to be uniform. However, it might not be the scenario as the basin is as large as 1246 square km. On the contrary, flood map produce from the calibrated model was comparable to satellite-based map. This has ensured the confidence on the calibrated hydrologic parameters (Table 3.3, 3.4, 3.5).

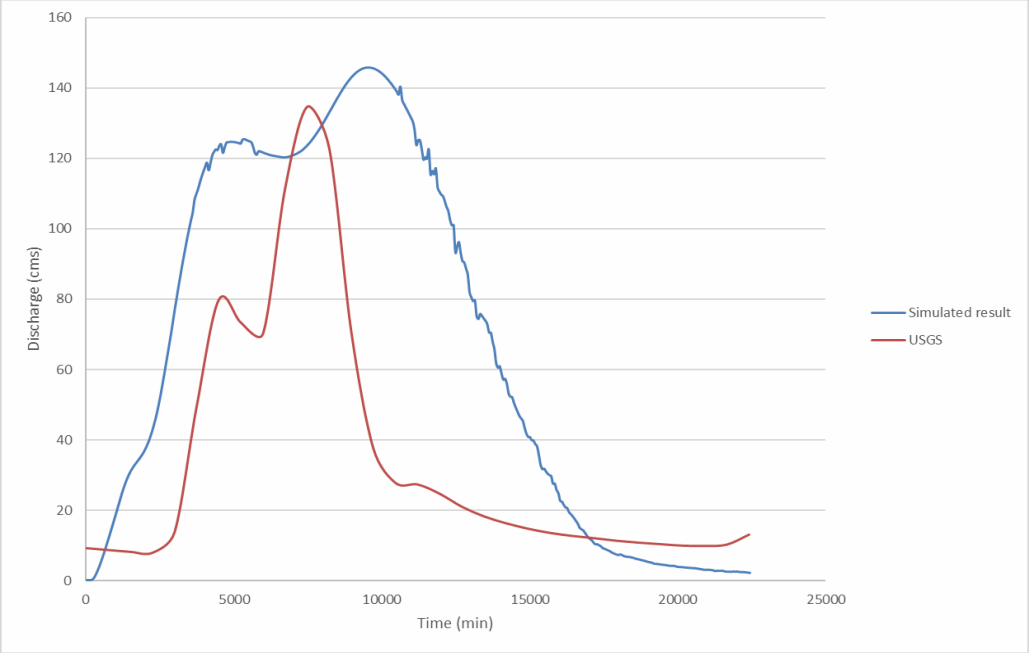

Figure 3.5: Simulated and observed hydrographs at the outlet of the watershed (USGS gage 02479300)

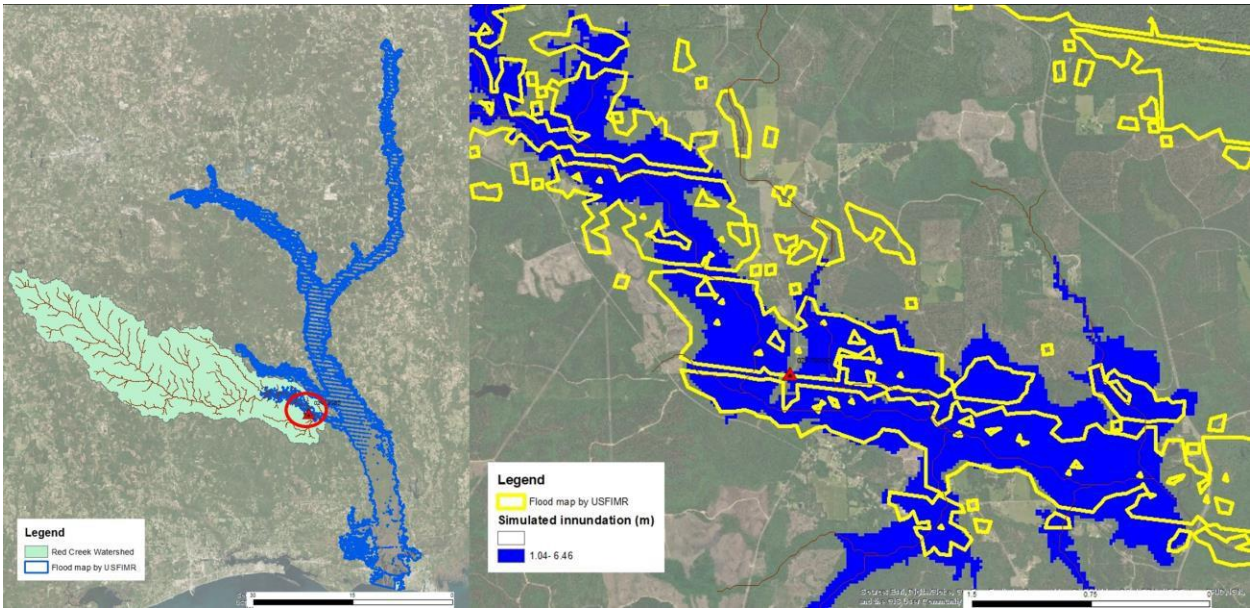

Figure 3.6: Validation- Flood map comparison (right); Flood map by USFIMR (left)

3.2.4 Simulation in GSSHA

The calibrated hydrologic parameters were used to simulate all the models. A total of 6 simulations were initiated for comparison: three reoccurrence interval storms, each using NED DEM and Modified DEM. Overall no of time steps was fixed for all the simulations according to rainfall data duration. Time step is one of the most important contributing factors to the model performance. (Ogden et al. n.d.) To minimize the computational expense in terms of time and secure integrity of required output a time step of 60 seconds was fixed as the time step. For all the simulations calibrated values (Table 3.3, 3.4) was used.

Table 3.3: Calibrated values for Manning's roughness for different land cover type

LU code	Land use	Manning's n
11	Residential	0.01155
12	Commercial and Services	0.0126
13	Industrial	0.0126
14	Transportation, communications and servi	0.01155
17	Other urban or built-up land	0.01155
21	Cropland and pasture	0.03675
22	Orchards, groves, vineyards, nurseries..	0.03675
23	Confined feeding operations	0.03675
24	Other agricultural land	0.03675
32	Shrub-brushland rangeland	0.0535
41	Deciduous Forest	0.107
42	Evergreen Forest	0.1605
43	Mixed Forest	0.107
53	Reservoirs	0.01177
61	Forested wetland	0.0624
75	Strip mines, quarries and gravel pits	0.01144
76	Transitional areas	0.01144
51	Streams and Canals	0.0364
62	Nonforested Wetlands	0.104

Table 3.4. Calibrated infiltration parameters

Infiltration parameter	values
Hydraulic conductivity(cm/hr)	0.0732
Capillary head (cm)	30.78
Porosity (m^3/m^3)	0.449
Residual saturation ((m^3/m^3)	0.112
Field capacity (m^3/m^3)	0.42
Wilting point (m^3/m^3)	0.251

CHAPTER 4

RESULTS AND DISCUSSIONS

4.1 Qualitative comparison of flood maps based on the three storms events

A qualitative comparison of the three storm events is presented herein. The simulation with the 46 years recurrence interval (Tr) resulted in the most extensive inundated area in comparison to the other events (for both without and with bathymetry; Figure 4.1, 4.2 respectively). This is expected due to the intensity associated with the rainfall occurrence that governs this storm event. Tr 26 and Tr 2 also yielded considerable inundation extents, comparable to their rainfall intensities. However, while comparing 4.1 and 4.2 a noticeable change in flooded extent at certain areas (inset maps in Figure 4.1 and 4.2) of the watershed. In 4.1 there is not much visual change in Tr26 and Tr46 induced flood extent but in 4.2 changes are visible. This strengthens our hypothesis that incorporation of bathymetry will produce more accurate results.

Concurrently, an estimation of the outlet discharges for each of the six simulations presented with proportional results (Figure 4.3) to the intensities of rainfall recorded for said events. Due to conservative simulation time, produced hydrograph is discrete and limited to daily output. Tr2 showed the most difference in magnitude while comparing the instantaneous daily discharge. With the increase in daily rainfall intensity Tr2 hydrographs had a higher magnitude for NED than the Modified DEM. For Tr26 there was no particular trend in increase or decrease of the discharge. Tr46 showed a continuous trend of higher magnitude for the Modified simulation result. In a watershed water travels from the farthest point to the outlet while going

through different hydrologic processes like evapotranspiration, infiltration, groundwater flow and so on. Thus, outflow at the watershed outlet depends on different hydrologic processes rather only on the geometric information of the streams.

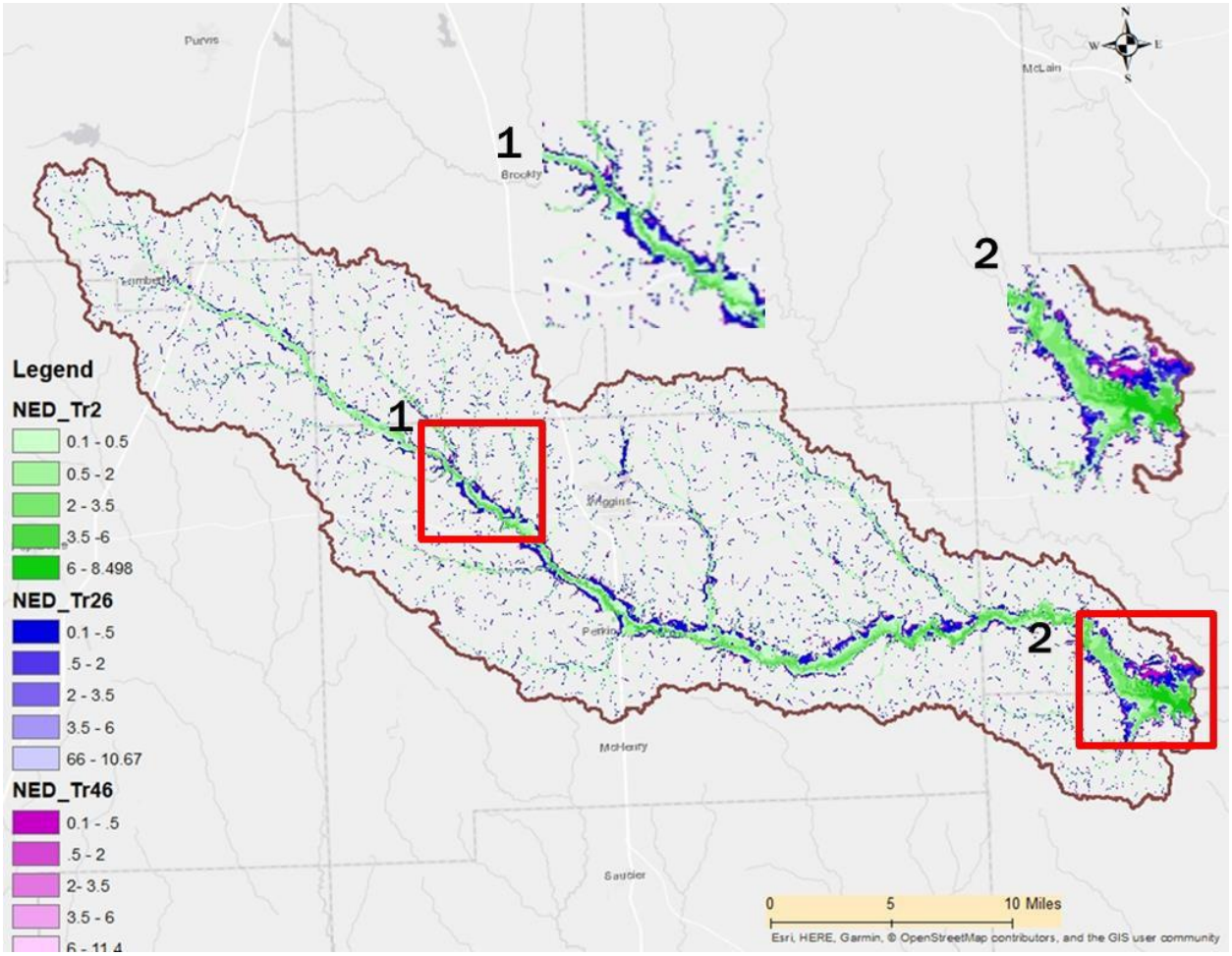

Figure 4.1 Map comparing flooding due to three storms events for without bathymetry

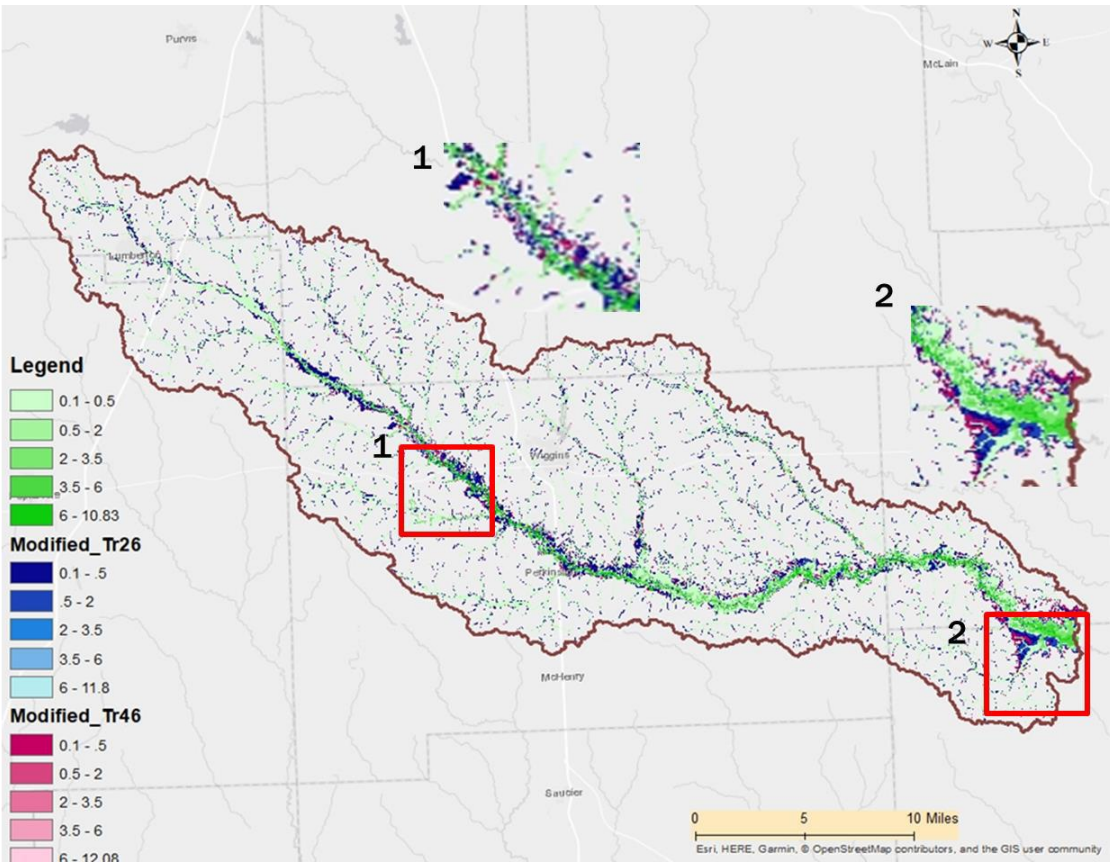

Figure 4.2: Map comparing flooding due to three storms events for with bathymetry

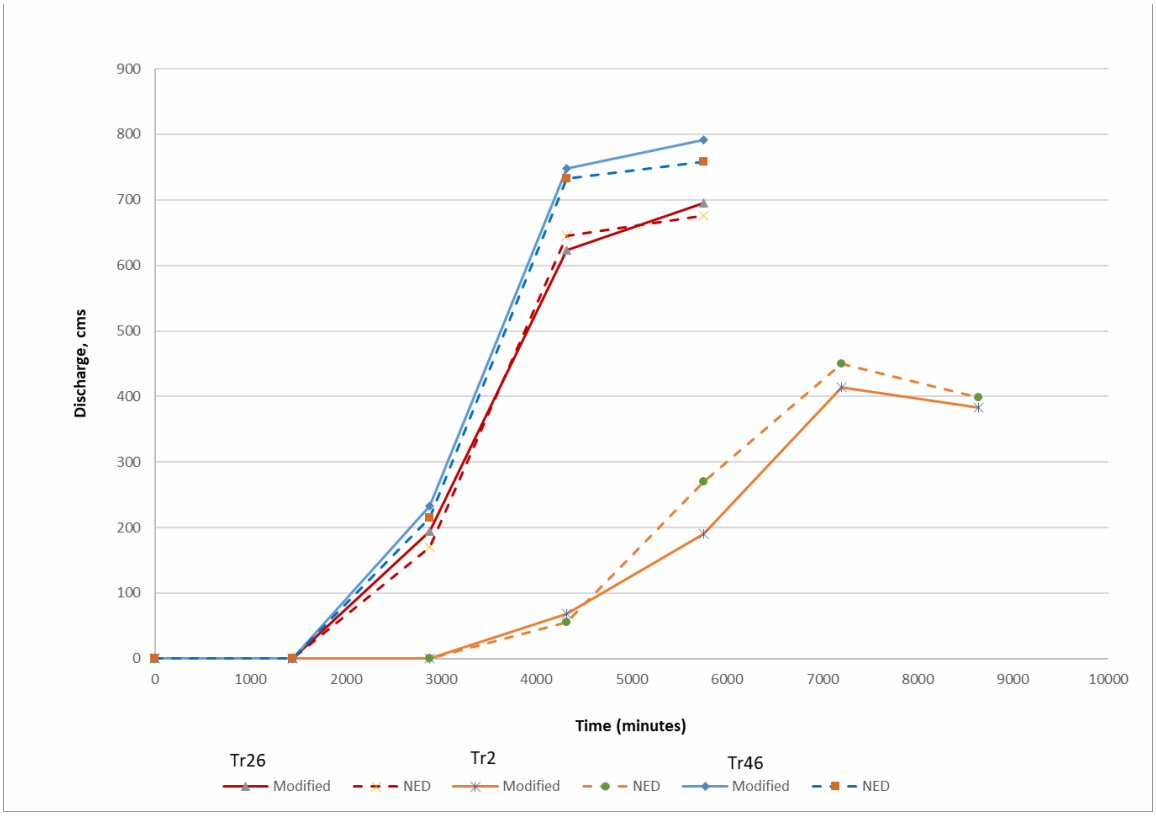

Figure 4.3 Outlet hydrograph comparison for the six simulations

Figure 4.4 through 4.6 depicts the comparison between the inundation extents for different storms with and out bathymetry incorporation. An evaluation of Tr 46 (Figure 4.4) shows that the downstream areas of the watershed depict less inundation when bathymetry data is incorporated in comparison to the no-bathymetry scenario (In Figure 4.4, Inundation_NED is seen beyond the extents of Inundation_Modified in the downstream areas). On the contrary, inundation of the upstream areas of the watershed is less influenced by the with/out bathymetry-condition analyses. Figure 4.5, in which the inundation extents of Tr 26 is compared, also is akin to Tr 46. This is probably due to the reason that all the water from upstream is drained towards the outlet making the flooding prominent where most of the water is. Inset maps show areas where significant inundation occurred. Interesting observations are elucidated from the analysis

of Tr 2 (Figure 4.6). Unlike Tr 46 and Tr 26, the mid-section of the watershed is entirely dominated by the inundation extent simulated without bathymetric data (i.e. increase in Inundation_NED in the midsections of the watershed). Naturally there is less volume of water during a smaller event, so it takes more time to reach the outlet. Thus, this may be ventured that to locate the flooded area near the outlet for a smaller magnitude storm event the simulation has to be run for a longer period of time.

Although visual interpretation is difficult due to the scale of the watershed and size of the streams, variations are prominent in certain areas of the watershed (inset maps in Figure 4.3-4.5). The cell size of the model domain is also a contributing factor for confounding visual results. To conclude the change accurately visual interpretation is not enough. A thorough quantitative analysis of inundates cells for each map for with/ out bathymetry is needed.

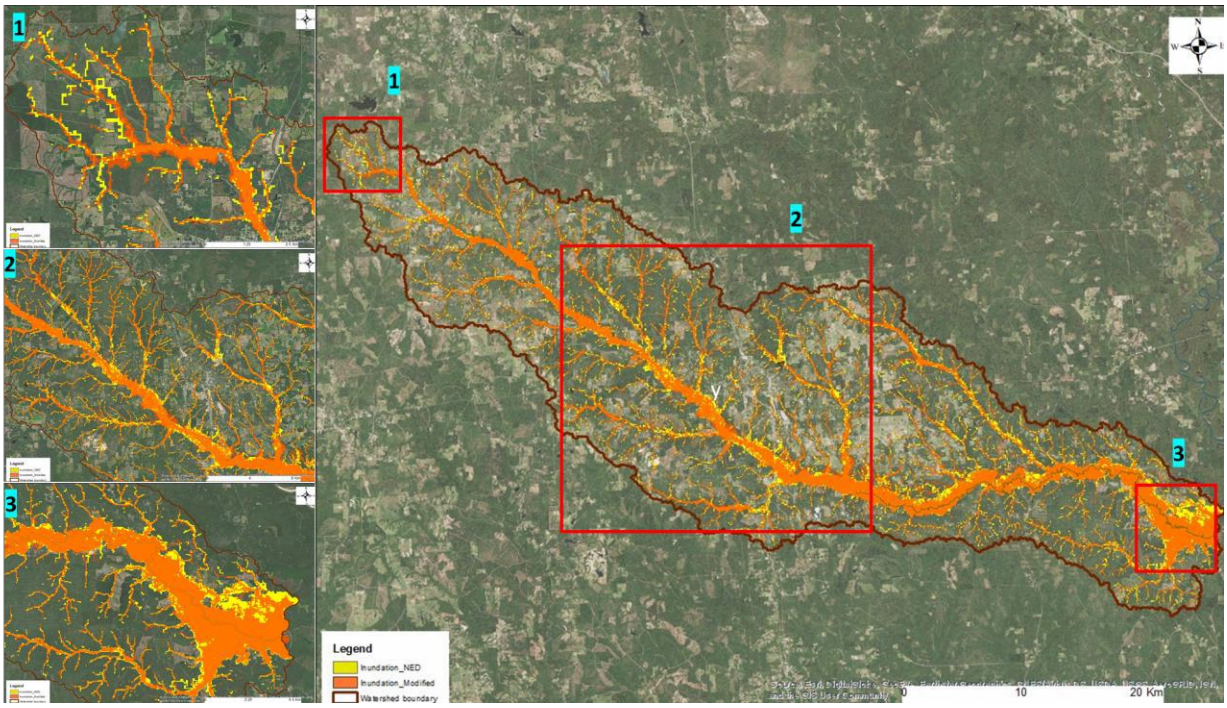

Figure 4.4: Inundation map overlay with and without bathymetry for Tr 46

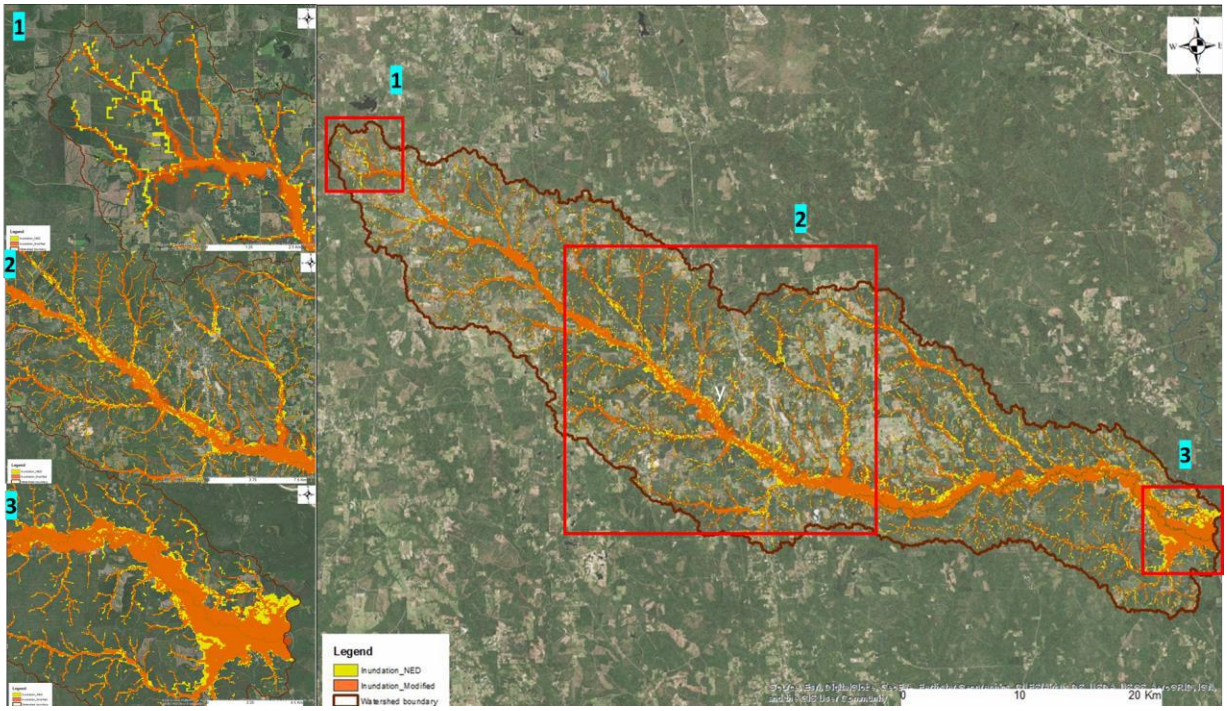

Figure 4.5: Inundation map overlay with and without bathymetry for Tr 26

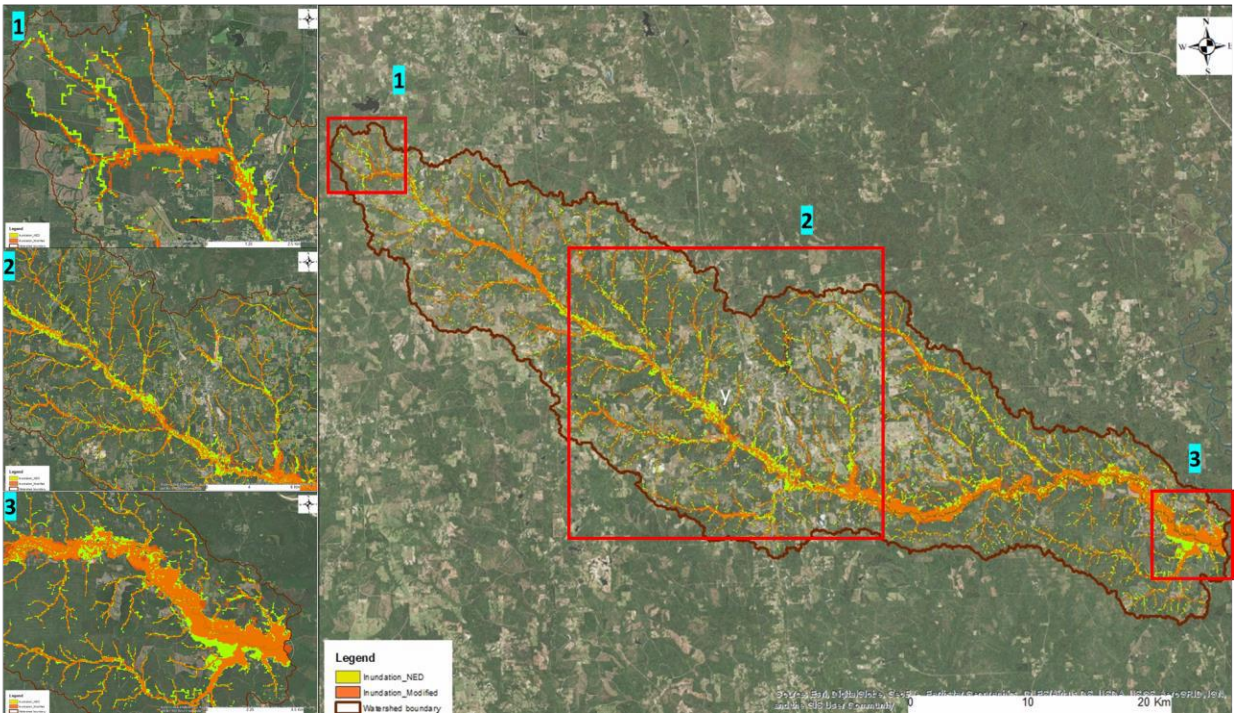

Figure 4.6: Inundation map overlay with and without bathymetry for Tr2

4.2 Quantitative comparisons

4.2.1 : Analysis of outlet hydrograph

The simulated discharge at the outlet has been quantitatively compared to each other (with/ out bathymetry) for every storm intensity using percent bias (PBIAS) objective function. PBIAS provides an estimate of the magnitude of % change between the discharge from with and without bathymetry models. In Moriasi et al. (2007) PBIAS has been used as an objective function in the statistical analysis of hydrologic data. Analyzing PBIAS (Eq. 4.1) one can have a sense of the average tendency of a set of data being larger or smaller than another set of data. Equation 4.1 calculates the PBIAS between outlet discharge from with/ out bathymetry models. Here $Q_{Modified}$ is the simulated discharge for with bathymetry model and Q_{NED} is the simulated discharge for without bathymetry model.

Zero is an optimal value indicating no change at all; positive and negative values show model overestimation and underestimation subsequently. PBIAS is expressed as a percentage. Table 4.1 shows the PBIAS for different storm intensity. The values range from 1.3 to 10.1% which suggests that the difference is not drastic in terms of outlet discharge. Tr2 has a negative value which means discharge produced by “without bathymetry” model was larger than “with bathymetry” model. Comparison among the PBIASs for different storm events suggests that Tr2 produced the highest difference due to likely the simulation duration. Tr26 and Tr46 showed very little PBIASs almost close to zero. During a large event there is more area flooded compared to a smaller event whether it is with or without bathymetry. It has already been anticipated that during a large event the change is minimal while using bathymetry data. The minimal change in hydrograph also shows agreement with the speculation made earlier. Also, another aspect to be considered is that all the hydrographs (Figure 4.6) have only the rising limb due to shorter simulation duration, the only hydrograph for Tr2 has a slightly longer duration

allowing the hydrograph to start forming the recession limb.

$$PBIAS = 100\left(\frac{\sum(Q_{Modified} - Q_{NED})}{\sum Q_{NED}}\right) \quad (5)$$

Table 4.1: PBIAS estimations for simulated hydrographs for with/ out bathymetry models

Storm Intensity	PBIAS %
Tr2	-10.19
Tr26	1.34
Tr46	3.83

4.2.2 : Inundation comparison for the entire watershed

The percentage of the watershed area that is inundated is graphed against the recurrence interval of the storm event (Figure 4.7). For each storm event, the differences between percentage inundated area based on a depth threshold, and inclusion/non-inclusion of bathymetry data have been portrayed. For a given storm event, gray and yellow bars depict the percent of the basin area that is inundated. A set of two bars per storm is known as a 'cluster' for ease of explanation, from this point onward.

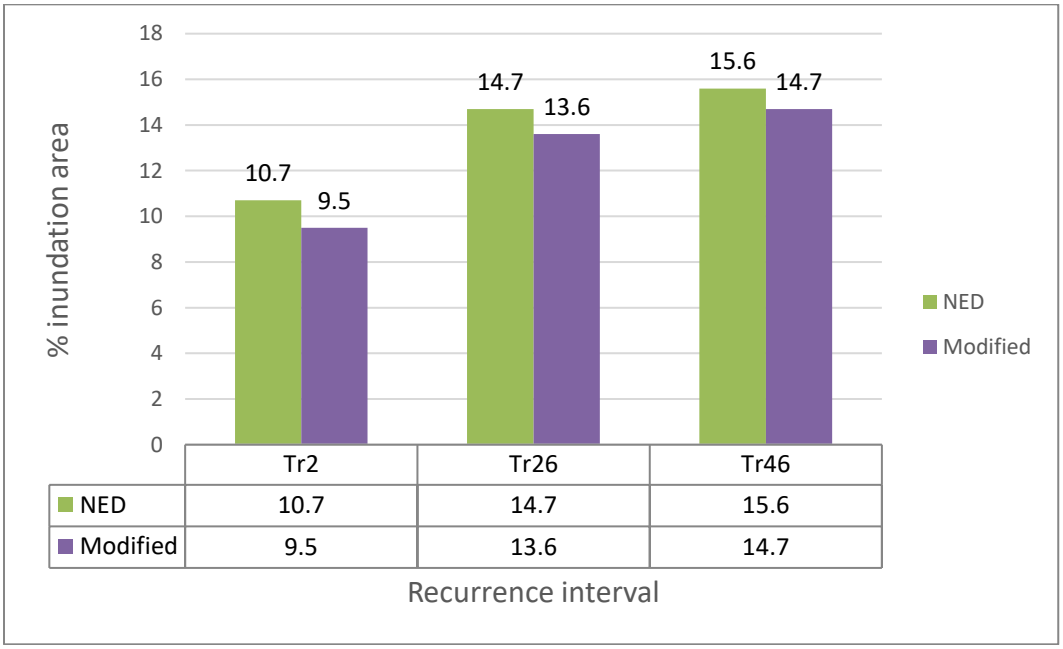

Figure 4.7: Percentage of the watershed that is Inundated for the six simulations

The increasing percentage areas of inundation (increase in height of each cluster with increasing recurrence interval of the storm events) shows that rainfall intensity governs the increment in flood stage regardless of whether river bathymetry calculations were not used in the analysis. This is attributed to the well-known relationship between rainfall intensity and river flood extent.

Comparing the percentage of flooded area is not enough to analyze the impact as there might be considerable overlap between the two models (with/ out bathymetry). Two different models can produce a very similar number of flooded cells but in different localized zones due to changes in elevation in stream bed as all the water propagation (1D and 2D overland) is due to elevation differences. To have a clear idea of the comparison between flood extent difference three different indices have been used: Fitness Index (F%), (Bates, P. D. & De Roo. 2004), Advance Fitness Index (AFI%) (used in Munasinghe et al., 2018) and Percent change (%change).

The F% gives the percentage of estimated inundated area (wet cells) which has been produced by both the models (with/ out bathymetry). A value of 100% corresponds to complete overlap between the models' (with/ out bathymetry) inundation area which indicates that there is no change due to the incorporation of geometric information. A 0% means that there is no overlap at all which is highly unlikely as the 2D overland flow must cross the same floodplain. The AFI% is a similarity index which depicts how much similar wet/ dry cells i.e. areas inundated/noninundated was predicted by both the models (with/ out bathymetry). % Change gives an idea of change in inundation produced for with bathymetry model with respect to without bathymetry model. Equation 4.2 to 4.4 calculates comparison indices. Here I_N and I_M are the simulated inundation; A_N and A_M are total simulated inundated and non-inundated area. Here, N and M denotes with (NED) and without (Modified bathymetry models.

$$F\% = 100\left(\frac{I_N \cap I_M}{I_N \cup I_M}\right) \quad (6)$$

$$AFI\% = 100\left(\frac{I_N \cap I_M + NI_N \cup NI_M}{A_N \cup A_M}\right) \quad (7)$$

$$\%\, Change = 100\left(\frac{I_N - I_M}{I_N}\right) \quad (8)$$

In Figure 4.10 all the quantitative indices have been graphed for the whole watershed with respect to storm scenarios. More than 50% of the inundated area intersected in the watershed which is very reasonable. As the storm intensity increases the percentage of overlap increases. Similarly, % change also shows the same trend. It can be anticipated that with increasing storm intensity the inundated area has increased so does the similarity in the inundated and non-inundated area. The AFI values suggest that there are almost 98% similar cells that have been predicted as flooded by both the models (with/ out bathymetry). This includes both inundated and non-inundated area. The number of non-inundated cells are higher than inundated

cells in the watershed which has governed the AFI estimates. This has produced a similar percentage for different storm scenario.

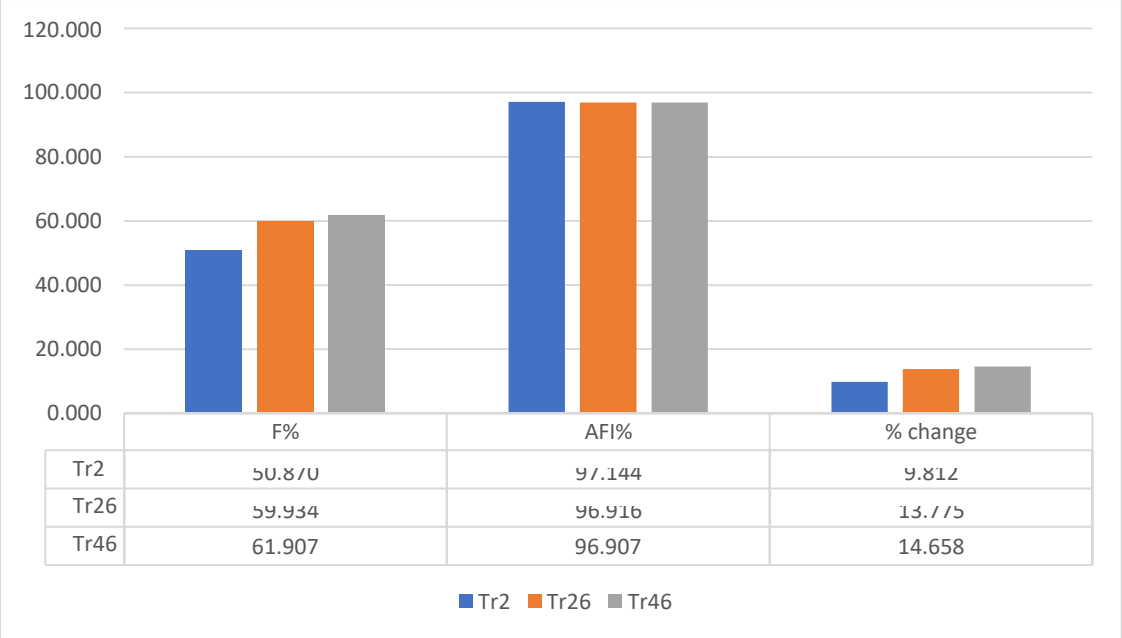

Figure 4.8: Comparison of diffent indices with respect to storm intensities

4.2.3 Comparison of inundation for different stream order

To compare the change in different streams, buffer areas were created around the streams (Figure 4.9). The buffer distance was fixed on the basis of the average width of the streams which was approximated from Google Earth imagery. As shown in the legend of Figure 4.9 the buffer distance was 100, 200, 300, 1000 and 1250 m for sub subsequently stream order one through five.

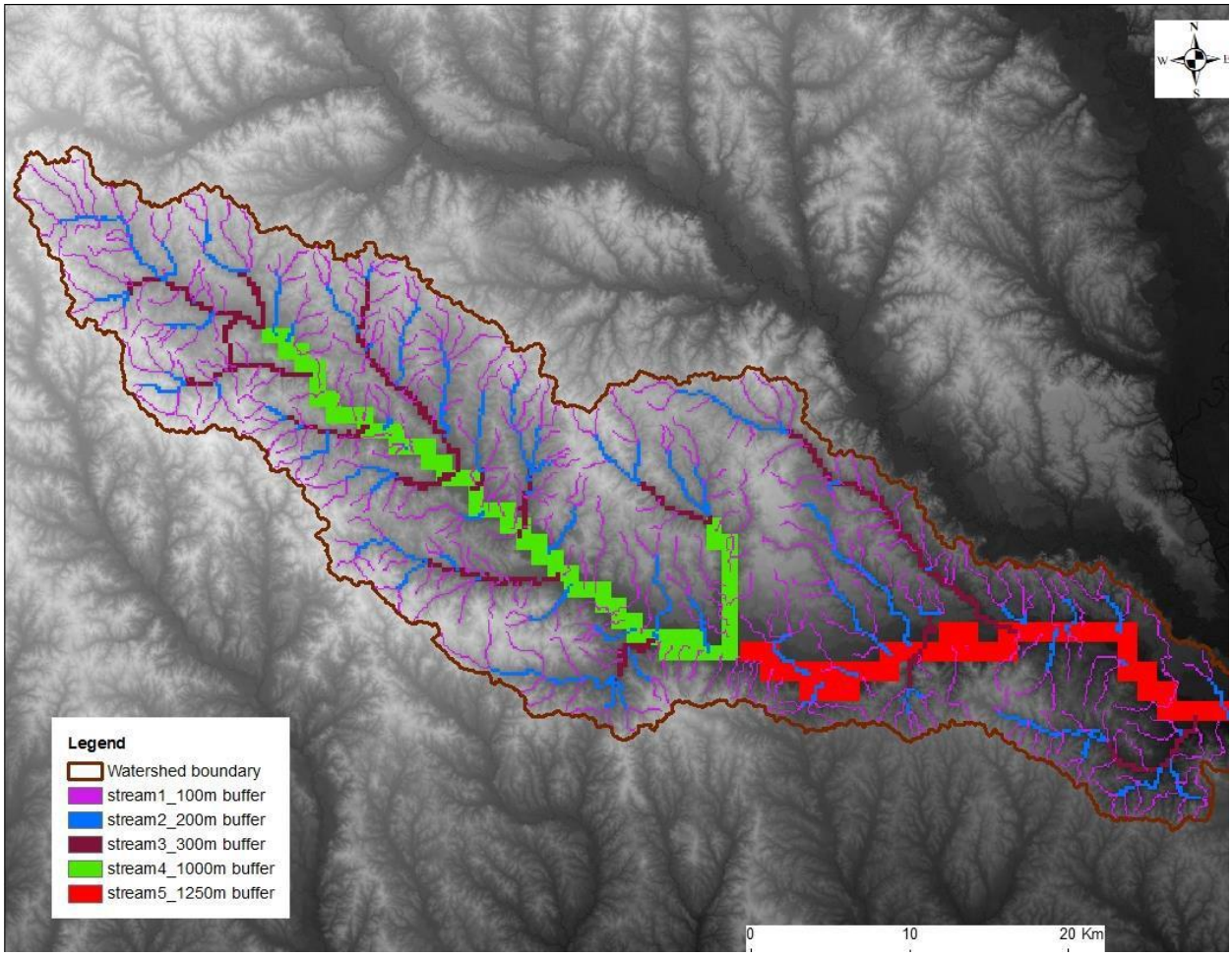

Figure 4.9: Buffered area for different stream order

Table 4.2 reveals all the comparison indices for different stream orders in the watershed which has graphed in series of figures from 4.10 to 4.13. Figure 4.10 shows a comparison of the indices for every stream order individually due to three storm intensity and figures 4.11 through 4.13 represents the comparison of the indices for the three storm intensities for all the stream orders. In Figure 4.10 a gradual increase in F% and AFI% can be located with an increase in storm intensity and % change shows a gradual decrease in all the stream orders except for stream order 5.

Table 4.2: Comparison indices for different stream order

	Stream order 1			Stream order 2			Stream order 3			Stream order 4			Stream order 5		
	F%	AFI%	% change	F%	AFI%	% change	F%	AFI%	% change	F%	AFI%	% change	F%	AFI%	% change
Tr2	50.35	78.62	6.31	57.54	75.53	4.64	57.39	75.75	17.07	46.52	81.96	23.15	66.70	84.97	11.10
Tr26	58.84	77.74	2.82	66.67	78.31	3.45	67.52	78.70	12.17	66.73	85.08	12.24	76.68	86.87	33.25
Tr46	60.35	77.82	2.92	68.34	78.96	2.51	69.85	79.78	11.65	70.49	86.16	8.67	79.59	87.90	9.76

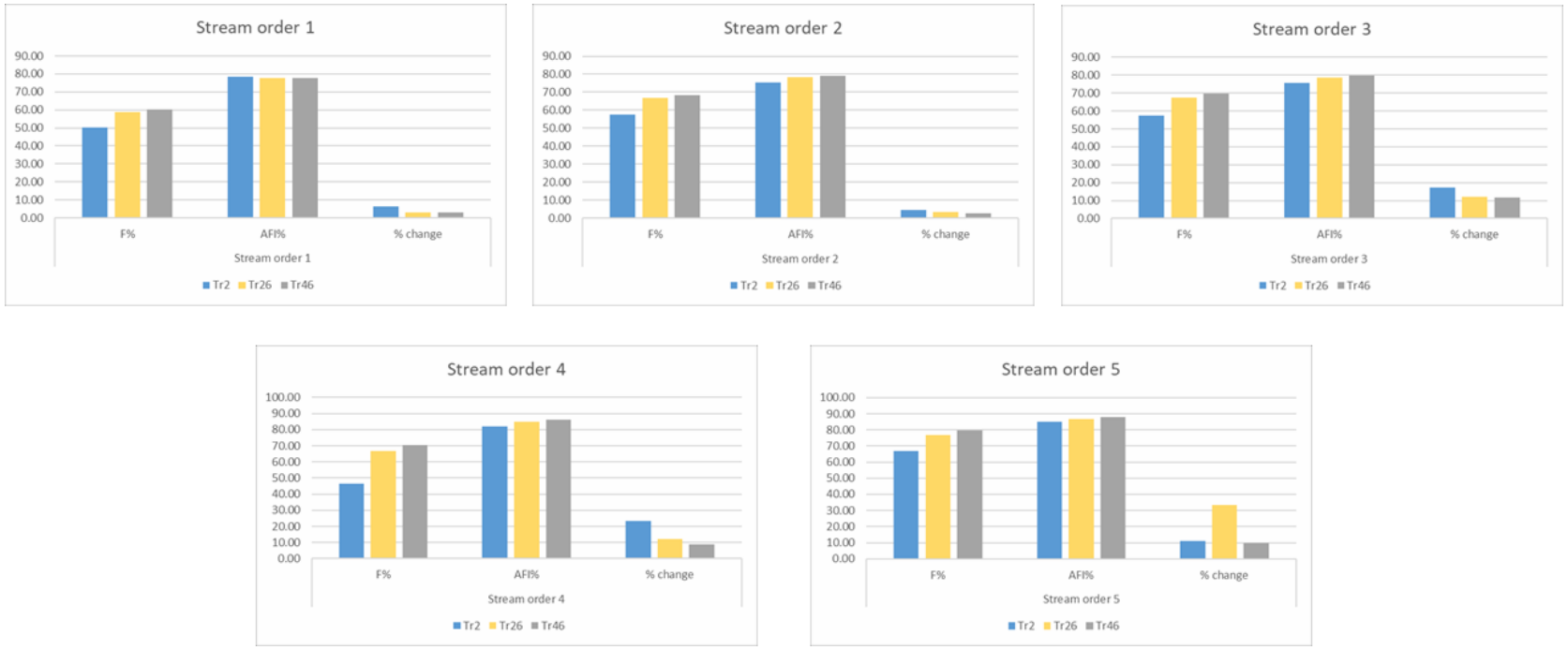

Figure 4.10: F% comparison for different stream order with respect to storm intensities

For a given stream order (1 to 4), F% gives the percentage of overlapped wet cells without any bias, so we can see that the percentage of overlap is increasing with storm intensity by flooding more common areas. AFI% has also shown a similar trend. However, the % change has a decreasing trend. This trend can be explained by assuming that during a large storm event regardless of bathymetry data a larger area is flooded making the change more minimal. This is because there are more common areas inundated/ non- inundated in the watershed when a large area of the flood plain is over flown with water. Another pattern to be noticed is that stream order 3 and 4 had a higher percentage of change compared to stream order 1 and 2, which suggests that comparatively larger (which is a medium sized river) streams in a medium sized watershed are more sensitive to bathymetry data than smaller streams. Thus, bathymetry data is important for accurately simulating flooding in medium sized streams.

While stream order 1 through 4 showed very similar and explainable results, stream order 5 represented a very interesting pattern in the %change. For Tr26 it showed the highest change and almost similar change for Tr2 & Tr46. This can indicate two important things (1) medium sized rivers are more responsive to bathymetry data, and (2) the effect of bathymetry is perceptible for a certain magnitude of the storm event. When the amount of water is much less it cannot travel beyond a certain area into the floodplain and there is not sufficient water to show much change. During a large flood like Tr46 changes due to bathymetry incorporation are minimal in flood extents.

In figure 4.11, a cluster of five bars shows the F% for five stream orders for a particular storm intensity. The percentage of overlap has the same trend for every storm intensity: with increasing stream order the percentage of overlap increases except stream order 4 has a drop in the overlapped estimate for all the storm scenarios addressing minimum overlap hence maximum

change due to bathymetry incorporation. This can be due to the reason that comparatively smaller and larger streams are less affected due to the bathymetry incorporation. This is indicating towards the hypothesis made earlier that Stream order 4 being a medium sized stream even for a medium sized watershed showed a larger difference. AFI% in figure 4.12 does not possess unusual patterns for varying storm intensities.

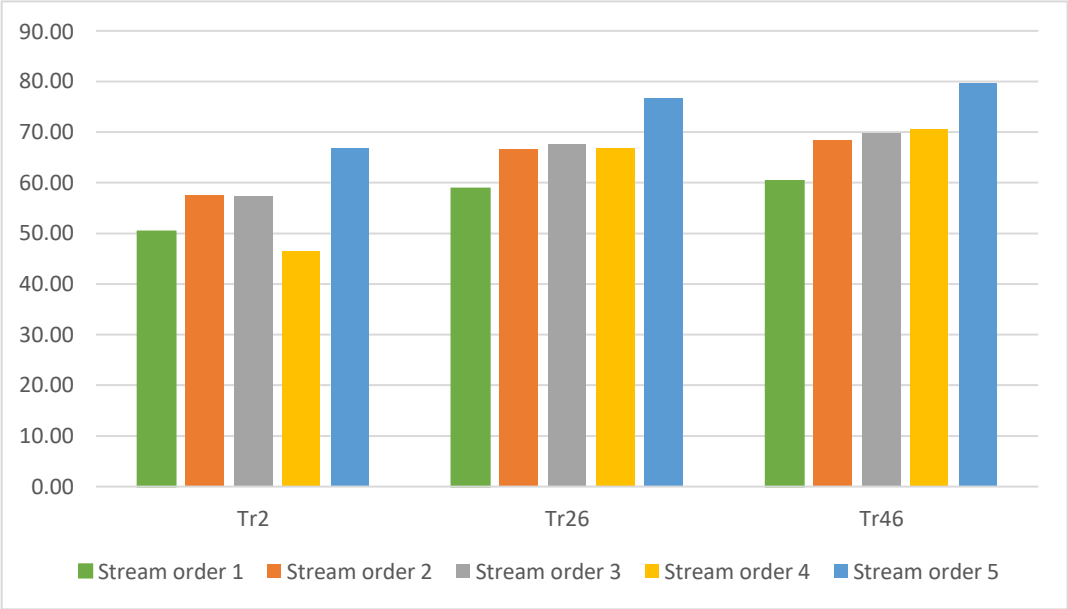

Figure 4.11: F% comparison for different stream order with respect to storm intensities

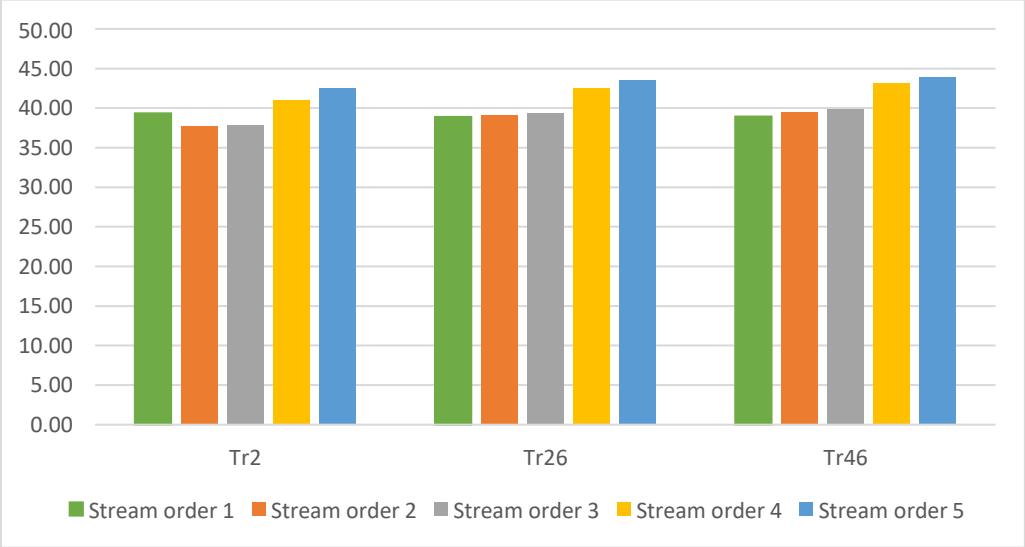

Figure 4.12: % Change comparison for different stream order with different storm scenario

Figure 4.13 depicts the comparison of % change for 5 stream orders showing the most interesting patterns. As a whole, stream order one and two were the least affected due to the incorporation of bathymetry. This validates part of the hypothesis that the smaller streams will not be affected significantly. In these small reaches, the difference between the with and without bathometry was highest for Tr2 meaning that larger storms will overwhelm the stream and its floodplain and so incorporation of bathymetry data is not significant. Stream order 3, 4 and 5 showed very different characteristics for varying storm intensity. Which is, for Tr2, 26 and 46 the highest affected streams are subsequently streamed order of 4, 5 and 3. Stream order 3, the average size stream for this watershed, is following a downward trend with increasing rainfall intensity. Stream order 5 has the highest value of 33% for the storm event Tr26 and for stream order 4 it is 23% for Tr2 which the second most affected stream order. Overall all the stream order showed the minimum response for the largest storm event Tr46.

There is an interesting synergy between the F% (overlap) and % change indices. For stream order 1, 2, 3 and 4 there is a gradual trend for all the indices. While in increasing storm intensity the overlap is increasing % change has decreased accordingly. For Tr2, stream order 4 has the least overlap while showing maximum %change. When compared among the three storm events all the stream orders showed some gradual and comparable indices except for stream order 5. Instead of having a gradual trend in overlap and similarity indices for different storm magnitude stream order 5 has the highest % change value for Tr26 which can be an indication of the idea that medium sized rivers are more sensitive to bathymetry data during a medium sized storm event.

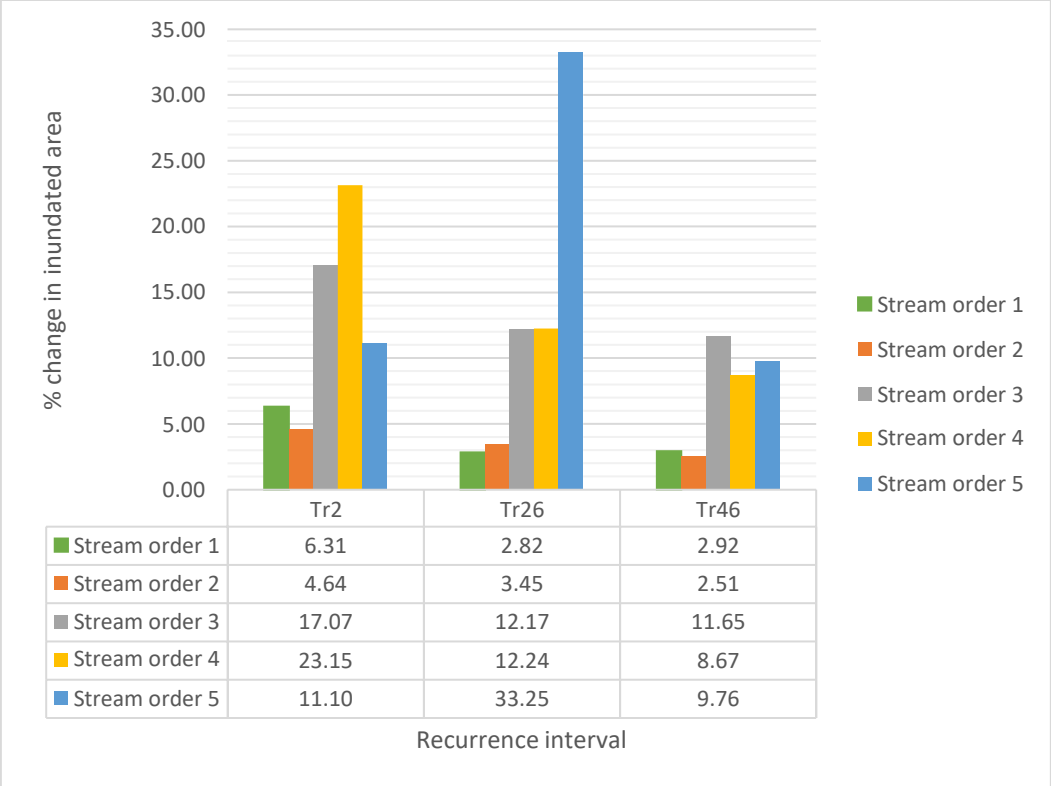

	Tr2	Tr26	Tr46
Stream order 1	6.31	2.82	2.92
Stream order 2	4.64	3.45	2.51
Stream order 3	17.07	12.17	11.65
Stream order 4	23.15	12.24	8.67
Stream order 5	11.10	33.25	9.76

Figure 4.13: % Change comparison for different stream order with different storm scenario

CHAPTER 5
CONCLUSION

The overall process of simulating a flood inundation map needs thorough assessments of the effect of the geometric representation of rivers. This study investigated the response of hydraulic simulation to the incorporation of hydraulic geometry derived river bathymetry using GSSHA, a distributed 2D hydrologic/hydraulic model. The inundation extents of three observed storms were generated with and out bathymetric inclusion.

It was clear from the results that integrating bathymetry is important for hydraulic modeling but with a considerable degree of effect as a function of storm intensity and stream order. When compared by stream orders it can be safely inferred that smaller streams are less affected compared to larger streams. For larger stream orders, spatial and temporal resolution of rainfall data can be of substantial influence. The inclusion of bathymetry in the analysis for a given storm event yielded an overall lower inundation percentage of the watershed. Exclusion of bathymetry yielded higher inundation, especially in the downstream areas of the watershed thus supporting the overarching hypothesis for this research that bathymetry data incorporation has a significant effect on flood simulation.

The results showed that smaller stream orders are less affected by the incorporation of bathymetry data compared to larger stream order. Stream order 5, the largest stream order for this particular watershed, had the most varying response to the inclusion of bathymetry data for different storm magnitudes which support to one of the hypothesis that medium sized streams will be more affected by inclusion/ exclusion of bathymetry data. Another important finding

from this study is that in contrast with the medium sized river a medium sized storm makes more difference than a smaller or larger event. This is because for a larger event a the floodplains are near fully flooded, unlike smaller event in which inclusion of bathymetry can make a considerable difference for the extent of flooding.

In conclusion, integrating bathymetry is important while simulation hydrologic and hydraulic models for flood prediction. As stated earlier, stakeholders and researchers require accurate assessment of flood intensity in terms of extent and depth which evidently is affected by the exclusion of bathymetry data. Future studies should focus on investigating how the difference in inundation varies with changing spatial resolution and scale of the watershed containing more classes of stream orders. Due to the computational time constraint in GSSHA in this study, long term rainfall events were not simulated. Future studies should also focus on longer storm events, perhaps using a more computationally efficient model to optimize run time. This will open a window for researchers to explore few more questions raised by this study.

REFERENCES

Bates, P. D., & De Roo, A. P. J. (2000). A simple raster-based model for flood inundation simulation. Journal of Hydrology, 236(1–2), 54–77. https://doi.org/10.1016/S0022 1694(00)00278-X

Bieger, K., Rathjens, H., Allen, P. M., & Arnold, J. G. (2015). Development and Evaluation of Bankfull Hydraulic Geometry Relationships for the Physiographic Regions of the United States. Journal of the American Water Resources Association (JAWRA), 1–17. https://doi.org/10.1111/jawr.12282

Cook, A., & Merwade, V. (2009). Effect of topographic data, geometric configuration and modeling approach on flood inundation mapping. Journal of Hydrology, 377(1–2), 131 142. https://doi.org/10.1016/j.jhydrol.2009.08.015

Dalrymple, T. (1960). Flood-Frequency Analyses. Manual of Hydrology Part 3. Flood-flow techniques. Geological Survey Water-Supply Paper, 1543–A, 80. Retrieved from http://pubs.usgs.gov/wsp/1543a/report.pdf

Downer, C. W., & Ogden, F. L. (2006). Gridded Surface Subsurface Hydrologic Analysis (GSSHA) User' s Manual Coastal and Hydraulics Laboratory Gridded Surface Subsurface Hydrologic Analysis (GSSHA) User' s Manual, (September).

Dudley, R. W. (2004). Hydraulic-Geometry Relations for Rivers in Coastal and Central Maine. United States Geological Survey, Coastal and Central Maine Scientific Investigations Report 2004-5042.

Dutta, D., Herath, S., & Musiake, K. (2000). Flood inundation simulation in a river basin using a physically based distributed hydrologic model. Hydrological Processes, 14(3), 497–519. https://doi.org/10.1002/(SICI)1099-1085(20000228)14:3<497::AID-HYP951>3.0.CO;2U

EPA. (2015). Climate Change in the United States: Benefits of Global Action. United States Environmental Protection Agency, Office of Atmospheric Programs, EPA 430-R-15-001. Retrieved from www.epa.gov/cira.

Gao, J. (2009). Bathymetric mapping by means of remote sensing: methods, accuracy and limitations. Progress in Physical Geography, 33(1), 103116. http://doi.org/10.1177/0309133309105657

Hammersmark, C. T., Fleenor, W. E., & Schladow, S. G. (2005). Simulation of flood impact and habitat extent for a tidal freshwater marsh restoration. Ecological Engineering, 25, 137 152. https://doi.org/10.1016/j.ecoleng.2005.02.008

Horritt, M. S., & Bates, P. D. (2001). Effects of spatial resolution on a raster based model of flood flow. Journal of Hydrology, 253(1–4), 239–249. https://doi.org/10.1016/S0022694(01)00490-5

Horritt, M. S., & Bates, P. D. (2002). Evaluation of 1D and 2D numerical models for predicting river flood inundation. Journal of Hydrology, 268(1–4), 87–99. https://doi.org/10.1016/S0022-1694(02)00121-X

Li, Z. & Clark, E., (2017). Development of large scale riverine terrain-bathymetry dataset by integrating NHDPlus HR with NED, CoNED and HAND data. American Geophysical Union Fall Meeting, New Orleans, Louisiana, December 11 – 16, 2017.

Li, Z., Mashriqui, H & Clark, E., (2017). Development of large scale terrain-bathymetry dataset for stream networks. 2017 Esri Water Conference, Orlando, Florida, February 7- 9 , 2017. (Presentation: slide 6)

Legleiter, C. J., & Overstreet, B. T. (2012). Mapping gravel bed river bathymetry from space. Journal of Geophysical Research, 117(F04024). http://doi.org/10.1029/2012JF002539

Leopold, L. B., & Maddock, T. (1953). The Hydraulic Geometry of Stream Channels and Some Physiographic Implications. Geological Survey Professional Paper 252.

Martini, F., & Loat, R. (2007). Handbook on good practices for flood mapping in Europe. European Exchange Circle on Flood Mapping, 60. https://doi.org/10.1016/j.cageo.2011.11.027

McKean, J., Tonina, D., Bohn, C., & Wright, C. W. (2014). Effects of bathymetric lidar errors on flow properties predicted with a multi-dimensional hydraulic model. Journal of Geophysical Research : Earth Surface, 119, 644–664. http://doi.org/10.1002/2013JF002897

Mishra, A., Anand, A., Singh, R., & Raghuwanshi, N. S. (2001). Hydraulic modeling of kangsabati main canal for performance assessment. journal of irrigation and drainage engineering, 127(1), 27–34. Retrieved from http://ascelibrary.org/doi/pdf/10.1061/(ASCE)0733-9437(2001)127:1(27)

Moore, M. R. (2011). Development of a high-resolution 1D/2D coupled flood simulation of Charles City, Iowa. Retrieved from http://ir.uiowa.edu/etd/1032

Tayefi, V., Lane, S. N., Hardy, R. J., & Yu, D. (2007). A comparison of one- and two-dimensional approaches to modelling flood inundation over complex upland floodplains. Hydrological Processes, 21(23), 3190–3202. https://doi.org/10.1002/hyp.6523

Yamazaki, D., Kanae, S., Kim, H., & Oki, T. (2011). A physically based description of floodplain inundation dynamics in a global river routing model. Water Resources Research, 47(4), 1–21. https://doi.org/10.1029/2010WR009726

Zhong, G., Liu, S., Han, C., & Huang, W. (2014). Urban Flood Maping for Jiaxing City Based on Hydrodynamic Modeling and GIS Analysis. Journal of Coastal Research, 68(2013), 168–175. https://doi.org/10.2112/SI68-022.1

Liu, J. (2005). Flood Control Dynamic and Introduction of Flood Hazard Maping in Japan. Hunan Water Resources and Hydropower, 2, 48-49.

Bowering, E.A. and Peck, A.M. (2014). A Flood Risk Assessment to Municipal Infrastructure Due to Changing Climate Part I: Methodology. Urban Water Journal 11(1), 20-30.

Tripathi, R.; Sengupta, S.K.; Patra, A.; Chang, H., and Jung W.H. (2014). Climate Change, Urban Dvelopment, and Community Perception of an Extreme Flood: A Case Study of Vernonia, Oregon, USA. Applied Geography, 46, 137-146

Brocca L, Melone F, Moramarco T, Singh VP. (2009). Assimilation ofobserved soil moisture data in storm rainfall-runoff modeling. Journal of Hydrologic Engineering 14(2): 153 165.

Bieger, K., Rathjens, H., Allen, P.M., and Arnold, J.G. (2015), Development and evaluation of bankfull hydraulic geometry relationships for the physiographic regions of the United States. Journal of the American Water Resources Association, (JAWRA) 1-17.

Renard B, Kavetski D, Kuczera G, Thyer M, Franks SW. (2010). Understanding predictive uncertainty in hydrologic modeling: the challenge of identifying input and structural errors. Water Resources Research 46: W05521. DOI: 10.1029/2009WR008328.

Sharif, H. O., Sparks, L., Hassan, A. A., Zeitler, J., & Xie, H. (2004). Application of a Distributed Hydrologic Model to the Flood of Bull Creek Watershed, Austin, Texas. https://doi.org/10.1061/ASCE HE.1943-5584.0000228

Ogden, F. L., Downer, C. W., & Meselhe, E. (n.d.). U.S. Army Corps of Engineers Gridded Surface/ Subsurface Hydrologic Analysis (GSSHA) Model: Distributed-Parameter, Physically Based Watershed Simulations. Retrieved from https://ascelibrary.org/doi/pdf/10.1061/40685%282003%29376

Downer, C. W., & Ogden, F. L. (2006). ERDC/CHL SR-06-1, Gridded Surface Subsurface Hydrologic Analysis (GSSHA) User's Manual; Version 1.43 for Watershed Modeling System 6.1. Retrieved from http://www.dtic.mil/dtic/tr/fulltext/u2/a455335.pdf

http://www.maris.state.ms.us/HTM/DownloadData/Statewide.html

GSSHA. (2017) https://en.wikipedia.org/wiki/GSSHA

Eco- Logic Restoration Services, LLC. (2007). Red Creek watershed action plan. Land Trust for Mississippi Coastal Plain Spring 2007- Friends of Red Creek. http://ltmcp.org/wp-content/uploads/2015/01/Red-Creek_Watershed-Action-Plan.pdf

Moriasi, D.N.; Arnold, J. G.; Liew, M. W. Van; Bingner, R. L.; Harmel, R. D.; Veith, T. L. (2007). Model Evaluation Guidelines for systematic Quantification of Accuracy In Watershed Simulations. Trans.2007, ASABE 50 (3), 885–900.

Munasinghe, D., Cohen, S., Huang, Y.-F., Tsang, Y.-P., Zhang, J., & Fang, Z. (2018). Intercomparison Of Satellite Remote Sensing-Based Flood Inundation Mapping Techniques 1. https://doi.org/10.1111/1752-1688.12626

Federal Emergency Management Agency (FEMA). (2009). Flood insurance study- Stone County, Mississippi and incorporated areas. https://geology.deq.ms.gov/floodmaps/Projects/MapMOD/docs/28131C_FIS_Report.pdf